A review of the general aspects of radiofrequency ablation

Y. Ni,[1] S. Mulier,[2] Y. Miao,[3] L. Michel,[2] G. Marchal[1]

[1]Department of Radiology, University Hospital Gasthuisberg, Catholic University of Leuven, Herestraat 49,
B-3000 Leuven, Belgium
[2]Department of Surgery, University Hospital of Mont-Godinne, Catholic University of Louvain, Avenue du Dr. Thérass 1,
B-5530, Yvoir, Belgium
[3]Department of General Surgery, University Hospital of Nanjing Medical University, Guangzhou Road 300, Nanjing, China

Abstract

As an alternative to standard surgical resection for the treatment of malignant tumors, radiofrequency ablation (RFA) has rapidly evolved into the most popular minimally invasive therapy. To help readers gain the relevant background knowledge and to better understand the other reviews in this Feature Section on the clinical applications of RFA in different abdominal organs, the present report covers the general aspects of RFA. After an introduction, we present a simple definition of the energy applied during RFA, a brief historical review of its technical evolution, and an explanation of the mechanism of action of RFA. These basic discussions are substantiated with descriptions of RFA equipment including those commercially available and those under preclinical development. The size and geometry of induced lesions in relation to RFA efficacy and side effects are discussed. The unique pathophysiologic process of thermal tissue damage and the corresponding histomorphologic manifestations after RFA are detailed and cross-referenced with the findings in the current literature. The crucial role of imaging technology during and after RFA is also addressed, including some promising new developments. This report finishes with a summary of the key messages and a perspective on further technologic refinements and identifies some specific priorities.

Key words: Radiofrequency—Tumor ablation—Minimally invasive therapy—Review

Malignant neoplasm remains one of the most life-threatening challenges worldwide. Among conventional therapies, radiotherapy and chemotherapy interfere with the metabolic processes, such that malignant cells (and normal cells) are injured or die slowly, leaving ample chance for tumor recurrence and adverse systemic side effects. They are generally regarded as palliative therapies aimed at slowing tumor growth and extending survival. Until recently, the only curative option for patients who had malignant tumors has been radical surgery, which, under certain circumstances, may promptly and completely remove all the tumor cells from an otherwise healthy body and thus cure this deadly disease. Unfortunately, only a small proportion of patients who have cancer can benefit from surgical eradication because of unfavorable tumor location, staging or extent, limited organ functional reserve, and/or high operative risk. To seek breakthroughs in this context, a series of minimally invasive tumor ablation techniques have been developed. The ultimate goal is "one applicator insertion, one episode of energy delivery in one outpatient session resulting in cure." Instead of excising the entire tumor from the patient as in standard surgery, these new therapies instantaneously kill the tumor in situ by localized injection of chemicals such as ethanol and acetic acid or by intratumoral delivery of lethal energies to freeze or heat the tumor as in cryotherapy or thermotherapy. Whether a minimally invasive technique can achieve complete control of local disease depends largely on whether it can satisfy the same eradication principle the same way as surgery for a margin-negative resection, i.e., destroy the entire tumor plus at least a 10-mm peritumoral margin. Radiofrequency ablation (RFA) is preferred over other heat-mediated modalities such as interstitial laser thermotherapy and microwave coagulation because of its low invasiveness, simplicity, favorable cost effectiveness, and especially the potential for further refinement. The present report provides an overview on the more basic

Correspondence to: Y. Ni; *email:* yicheng.ni@med.kuleuven.ac.be

aspects of RFA as background information to the other more clinically oriented reviews in this Feature Section of *Abdominal Imaging*. After this general introduction, we present a straightforward definition of the energy applied in RFA, a brief historical review of the technical evolution, and a simple explanation about the mechanisms of action. These basic definitions are substantiated with a description of equipment used for RFA, including those commercially available and those under preclinical development. The unique pathophysiologic process of thermal tissue damage and the corresponding histomorphologic manifestations after RFA are detailed and cross-referenced with the literature. The crucial role of imaging technology in RFA is also addressed, including some promising developments. The report finishes with a summary of the key messages and a perspective on further technologic refinement.

Definition of the energy used for RFA

Radiofrequency (RF) is an electromagnetic wave frequency between audio and infrared that ranges from approximately 10^4 to 3×10^{12} Hz. RFA can be defined as destruction of biological tissues by using electricity from an unmodulated, sinusoidal wave, alternating current (AC) at an electromagnetic frequency that falls well into the range characteristic of radio broadcasting signals (e.g., 30–300 KHz for long wave, 300–3000 KHz for medium wave, and 3–30 MHz for short wave), but preferably around 5×10^5 Hz, or 500 KHz. This frequency is in the range of medium wave, i.e., high enough (>20 KHz) to cause molecular frictional heating without stimulating neuromuscular reaction and electrolysis and low enough (<20 MHz, far from microwave of 1–300 GHz) to confine energy transmission to a more controllable tissue mass without generating excessive radiation [1, 2]. AC stronger than 100 mA at a lower frequency of 50 Hz (household mains electricity) is known to cause fatal electrocution and ventricular fibrillation. In contrast to the ionizing electromagnetic waves at much higher frequencies such as the typical x-ray of 10^{18} Hz, the RF energy is non-ionizing and believed to be free of health hazards if used properly. The term *ablation* in the context of RFA can be comprehended as a kind of virtual surgical ablation, i.e., to devitalize a volume of tissue without removing it from the body, resulting in an effect similar to that of surgical resection.

Evolution of RF-based therapies

The use of electrical current to heat tissues for medical purposes is by no means new and can be traced back to the 19th century, shortly after the English physicist James C. Maxwell and the German physicist Heinrich Hertz theoretically and practically characterized electromagnetism. Near the end of the 19th century, the French scientist Jaques-Arsène d'Arsonval found that the neuromuscular response or electric shock did not occur when the frequency of AC passing through the body was set above 10^4 Hz. At approximately 1900, the Croatian physicist Nikola Tesla first recognized heating of biological tissues with RF current. The first widely accepted RF generator was produced in the early 1900 s through the collaboration of a physicist (William T. Bovie, 1882–1958) and a surgeon (Harvey Cushing, 1869–1939). Little has changed since the basic principles were applied by Bovie [1, 2]. These pioneering endeavors laid the foundation for the subsequent use of RF energy in medicine. During the development of RFA, although certain methodologic or conceptual differences might exist, several historical synonyms have been used for electricity-generated heat therapies, including arsonvalization [1], fulguration [3, 4], electrocoagulation [5], oscillatory desiccation [6], electrocautery [7, 8], electrosurgery [9, 10], diathermy [11], electrophysiotherapy [12], and RF coagulation [13].

For almost a century in clinical oncology, physicians from many disciplines have applied this technique to coagulate surface lesions such as skin tumors, lesions in accessible body cavities such as bladder, gastrointestinal, and tracheobronchial tumors, and lesions exposed at open surgery such as intracranial tumors [6–10]. Meanwhile, the "electric scalpel," an RF instrument, has widened the therapeutic scope of all surgical specialties by allowing the safe division of tissue and by coagulating bleeding vessels [9, 10]. In principle, these applications use a sharp, brief RF energy delivery linearly for a bloodless incision or at a focal point for coagulative hemostasis to minimize unwanted energy dissipation into the surrounding tissues and collateral damage [10]. Similarly, destruction of peripheral sensory nerves for control of constant pain [14] and transcatheter ablation of abnormal cardiac conducting pathways for the treatment of arrhythmia [15, 16] require more or less focused RF energy deposition.

In contrast, interstitial RFA for the management of solid malignancies necessitates a more dispersed distribution of relatively mild RF energy to cause a more extensive sphere of tissue destruction. In recent years, the RFA of deeply seated tumors in internal organs has been realized thanks to two important and associated technologic developments in the clinic: (a) the increased sensitivity and specificity of imaging diagnosis with advanced ultrasound (US), computed tomography (CT), and magnetic resonance imaging (MRI); and (b) improved guidance in and monitoring of interventional procedures with implementation of dedicated imaging modalities and endoscopic equipment. In accordance with this trend, tremendous efforts have been made mainly to remodulate the RF technology from previously more focused to currently more volumetric energy deposition to meet the requirements of oncologic radi-

cality for tumors of clinically relevant size. These advances have been achieved by upgrading RF generators to yield more appropriate power output (e.g., "pulsed" current depositions), controllable tip temperature, and impedance adaptation, by optimizing the RFA electrode configuration to improve heat generation and distribution, and by decreasing local heat loss through vascular occlusion and induced hypotension. These changes have significantly improved the efficacy of RFA and enabled ablation of larger lesions on the order of several centimeters [20–34] compared with only several millimeters previously [17–19]. Numerous groups and individuals have actively participated in this campaign of experimental research and instrumental optimization and jointly contributed to the current boom in RFA therapy [17–34]. Notably, even a few doctoral theses have focused on RFA-related topics [34–40].

Thus far, the liver is the major organ that has been studied most intensively for the management of primary and metastatic tumors [18, 23–25]. After many years of percutaneous ablation of small hepatocellular carcinomas (HCCs) in patients who had cirrhosis, Lencioni et al. demonstrated superior 3- and 5-year survival rates of 89% and 61%, respectively, and concluded that RFA is more effective than surgery and should be offered as the first-line treatment for patients who have HCC [41]. The evolution of this technology and increasing clinical experience have opened up new frontiers in treating, with encouraging results, tumors of other organs including the lung [42, 43], breast [44], brain [45], bone [46–50], adrenal gland [51, 52], prostate [53, 54], kidney [55–58], pancreas [59], spine [60], retroperitoneum [61, 62], and so on (there are too many publications to cover entirely). Experimentally, VX2 carcinoma (but not sarcoma as erroneously termed elsewhere [63]) is the most popular transplantable tumor model in rabbits. Until recently, this extremely malignant tumor was regarded as incurable [63]. However, with a modified VX2 tumor fragment implantation method (secured by sealing of the puncture with tissue glue), an eradication rate higher than 50% has been shown with RFA in the liver [64], kidney [65, 66], lung [67, 68], and brain [69] as proved by long-term tumor-free survival rates in animals and histomorphologic evidence [34, 64–69]. These new developments most likely prelude a fundamental shift in the way physicians traditionally approach cancers.

Mechanisms of RFA

The mechanisms of tissue heating in RFA are based on the adequate conversion of electrical energy into thermal energy. Most current RFA devices are monopolar, i.e., there is a single "active" electrode, with current dissipated at a returning grounding pad. During the RFA procedure, an electrode is inserted into the target tissue. RF current flows from the generator through the non-insulated tip of the electrode into the tissue and follows the natural paths in the interstitium toward the dispersive electrode or grounding pad to form an entire electric circuit. Under a certain voltage as the potential energy, electrons travel smoothly, without significant thermal effect, from one atom to the orbit of the next along that part of the circuit made up of metal conductors; the only poor conductors in this circuit are biological tissues with higher impedance. As the ions of the tissue attempt to follow the change in direction of the AC, ionic agitation occurs, resulting in frictional heat of the tissue, i.e., resistive or ohmic heating. Because the large surface area of the grounding pad prevents heat production by decreasing local current density and electrical resistance, the real frictional heat is generated and concentrated only in the immediate vicinity of needle electrode. Hence, it is the tissue around the electrode instead of the electrode itself that is the primary heat source in RFA. When the temperature increases to a certain level, normally higher than 70°C, instant tissue coagulation occurs. A similar type of tissue destruction can be created with bipolar RFA devices that have two "active" electrodes usually placed in close proximity, resulting mainly in destruction of the intervening tissues without the need of a grounding pad [20, 31].

Despite their distinct mechanisms, RFA can be conceptually confused with electrocautery [17, 18, 20]. Electrocautery uses an electrically heated tip to coagulate tissue and to control bleeding, whereas no RF current flows through the patient. The tip of the electrocautery device becomes heated by the passage of an electric current through a high resistance wire. When the heat is transferred from the tip by conduction to tissue for coagulation, i.e., conductive heat, several more focal and intense changes occur: cells vaporize, removing water from the tissue, thereby causing the tissue to shrink and the blood vessels to contract and/or the protein in blood cells and tissue to form a coagulum.

Biologically, the effects of heat-related therapies such as RFA on tissues including tumors involve multiple complex mechanisms and depend on the temperature and duration of heat exposure and on local factors such as organ perfusion, tissue density, and electrolyte concentration. Different characteristics of cellular damage are observed at different temperatures. Although variable among tissues, thermal injury begins at 42°C [70]. If the temperature is moderately increased to 42°C to 45°C for 3 to 50 h, as typically seen with hyperthermia (distinct from thermotherapy) [70], a progressive cellular degeneration similar to programmed cellular death or apoptosis occurs in steps of conformational change of macromolecules, damage to membranes, chromosomes and cytoskeletons, retardation of energy metabolism, nuclear pyknosis, and inhibition of DNA, RNA, and protein synthesis [71, 72]. However, even prolonged exposure at this temperature range will not kill all cells in a given volume because
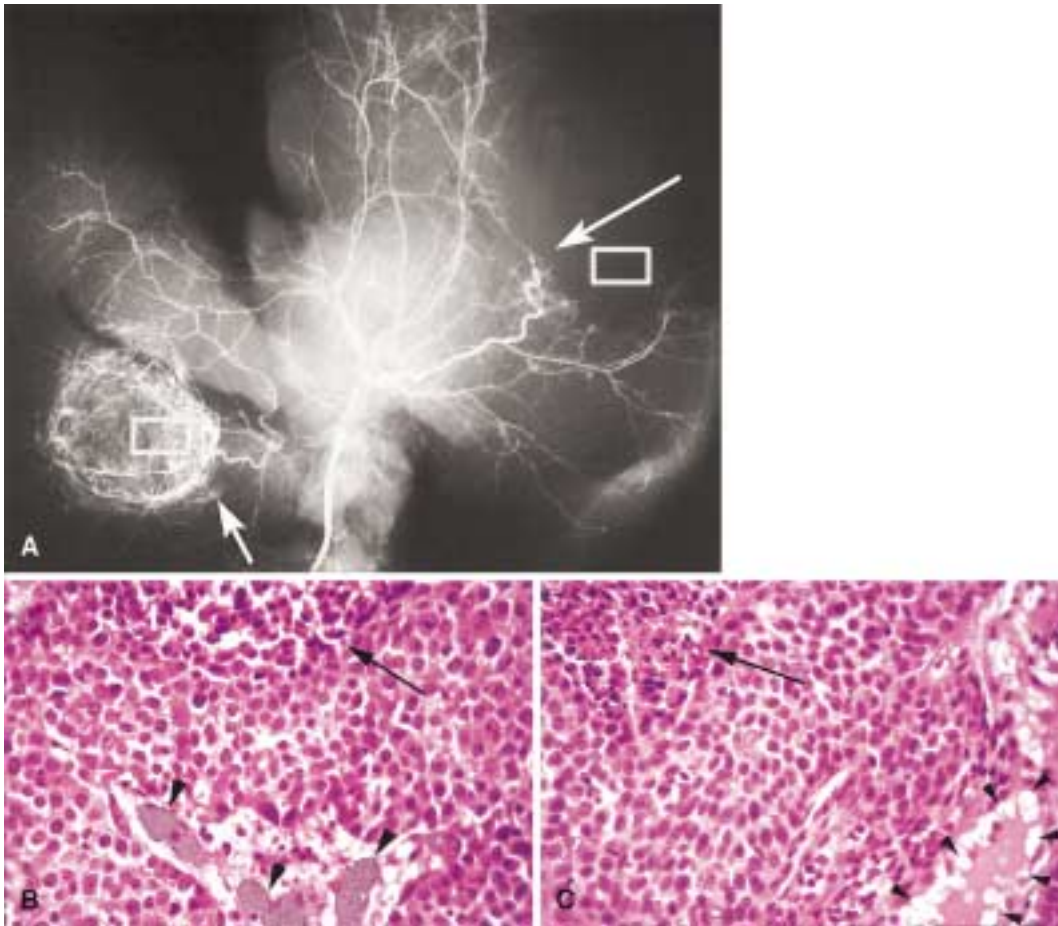
Fig. 1. Intraindividual comparison between the unablated and ablated VX2 tumors in the liver of a rabbit 1 day after RFA using a 5% saline mediated wet electrode. A Microangiogram displays an unablated hypervascular tumor in the right lobe of the liver with a tortuous afferent artery (small arrow) and an RF-ablated tumor in the left lobe seen as a filling defect with a truncated tumoral feeding artery (large arrow). The rectangular frames indicate the approximate locations where the histopathologic views (b and c) were obtained. B, C Photomicrographs of the (b) unablated and (c, right) ablated tumors display almost identical histopathologic appearances of the VX2 carcinoma in terms of tissue structure, cellular composition, and intratumoral spontaneous necrosis (arrow), i.e., thermal fixation or ghost phenomenon as seen in C. However, there is a remarkable distinction in the intratumoral vasculature. Viable tumor contains patent blood vessels (arrowheads) filled with blood cells (but now with injected barium particles for microangiography), whereas RF-ablated tumor contains nonfunctioning blood vessels filled with air bubbles due to heat-induced tissue coagulation and water evaporation (arrowheads). HE staining, original magnification 400×.

continued cellular function and tumor growth can be observed [73]. As temperature increases, the exposure time necessary for irreversible cellular damage shortens exponentially, e.g., exposure to 50.8°C for 2 min proves lethal to myocardial cells [73, 74]. At temperatures higher than 60°C, coagulation of proteins, which are basic constituents of cytosolic and mitochondrial enzymes and nucleic acid–histone complexes, instantaneously occurs, resulting in cellular death [75, 76]. However, temperatures higher than 100°C causes water in tissue to boil, vaporize, and carbonize, as is typically seen when dividing tissue and stopping hemorrhage with electrosurgery. Therefore, a temperature between 50°C and 100°C throughout the entire target volume is considered adequate for thermal ablation [77, 78]. Heat has a direct cytotoxic effect on the tumor and a considerable influence on tumoral vasculature. Vascular damage represents another important tissue response to thermal ablation. After heat exposure, the common histopathologic changes are microvascular cell swelling and disruption, intravascular thrombosis, and neutrophil adherence to venular endothelium. The observed decrease in microvascular perfusion during RFA and vascular shutdown after RFA (Fig. 1a–c) is probably the reason that RFA is superior to ethanol ablation [34, 64, 65, 67]. After RFA, progression of marginal vessel injury may lead to ongoing tissue necrosis. Aside from the thermal destructive effect of RFA, secondary anticancer immunity due to activation of tumor-specific T lymphocytes [79] appears to play a role in experimental RFA [64–69].

Biophysically, RF energy deposition in the tissue is governed by various factors including RF current density, current intensity, electrode size, tissue conductivity, and the duration and fashion of RF application. For a potential eradicative RF tumor ablation, i.e., the entire tumor plus a 1-cm peritumoral safety margin on all sides, the tumor size and corresponding required RFA lesion size (all assumed as spheres) are listed in Table 1.

To optimize the formation of a sizable RFA lesion, each of the following technologic developments, whether commercially available or under preclinical investigation, has been realized to deal with one or more of the biophysical factors mentioned above. These are explained from a practical point of view.

RFA electrodes: design and working principles

The first experiments with RFA on liver tissue were performed in 1990 by using plain electrodes [17, 80]. The transverse RFA lesion diameter was restricted to 0.6 to 1.7 cm in perfused pig liver [23, 80–85] due to a rapid increase in electric impedance with current shutoff, and the clinical results were disappointing [85–87].

Two mechanisms are responsible for impedance rise during RFA. The first mechanism is the irreversible dehydration and charring of the tissue immediately adjacent to the electrode [1, 77, 83, 88–90]. The second mechanism is the reversible formation of electrically insulating gas between the electrode and the tissue due to boiling and evaporation of tissue fluid [23, 81].

To overcome size limitations in RFA, numerous modified electrodes have been developed and tested since 1994. Some of the designed electrodes have been commercially available, and others are under preclinical investigation. Four different concepts have led to the development of five basic types of electrodes: bipolar (bipolar electrodes), saline perfusion through the electrode into the tissue (wet electrodes), internal cooling (cooled electrodes), and enlargement of the electric field (multiple and expandable electrodes).

Early electrodes

Bipolar electrodes

In bipolar RFA [20, 91, 92], a second parallel electrode is used instead of the dispersive plate. In monopolar RFA, the current density decreases as the inverse square of the distance from the electrode [93]. Because heating is proportional to the square of the current multiplied by the resistance (I^2R), heating decreases as the inverse of the fourth power of the distance in a very steep exponential decay [93]. Moreover, heating in this limited area is not homogeneous but concentric and preferentially takes places where it should not: immediately adjacent to the electrode, leading to rapid charring and power shutoff.

Table 1. Required RFA size in relation to tumor size

Tumor size in diameter (cm)	RFA size in diameter (cm)	RFA size in volume[a] (cm^3)
1	3	14
2	4	33
3	5	65
4	6	113
5	7	180
6	8	268
7	9	382
8	10	523

[a] $V = (\pi/6) D^3$, where V is spherical volume, π is the ratio of circumference to diameter, and D is diameter; RFA, radiofrequeney ablation

In contrast, in parallel bipolar RFA, there is a high and constant electric field gradient between the two electrodes, so that heating takes places homogeneously in the entire area between them [30]. With the electrodes separated by more than 2.5 cm in ex vivo liver, coagulation appears like a butterfly [20, 91]. Bipolar RFA was been abandoned after a short clinical trial in 1996 because of difficulties in correct parallel insertion by the percutaneous route [86].

Multiple electrodes

By applying current to multiple electrodes simultaneously, current is redistributed to a larger electrode–tissue contact surface. The current density is spread out more homogeneously over the covered area, which diminishes charring.

The simultaneous activation of multiple (two to five) parallel electrodes yields ellipsoid, triangular, rectangular, or spherical lesions, depending on the configuration, with a maximal diameter of 3.2 cm in ex vivo liver [94, 95]. When electrodes are spaced farther apart than 1.5 cm, the central area is not coagulated [94, 95]. The technique was abandoned because exact placement of the electrodes was difficult with a percutaneous approach [87, 96].

Current commercial electrodes (Table 2)

Wet electrodes

The wet electrode consists of a hollow electrode with one or more holes at the tip through which an isotonic or hypertonic (e.g., 5–36 %) saline solution is infused into the tissue, usually at a rate of 1 mL/min, and beginning 1 min before the start of RF coagulation [97–101].

Several mechanisms have been proposed to explain the increased coagulation diameter of a wet electrode. Some are due to the liquid (hydration), others to the salt (increased NaCl concentration), or both. The infused liquid fills the gap between the metal electrode and the tissue with highly conductive saline instead of electrically insulating gases [23, 64]. Saline infusion also allows

Table 2. Features of commercially available electrodes for radiofrequency ablation

| Company | Electrode | Type | In perfused pig liver, mean ± SD (range) | | Reference |
			Transverse diameter (cm)	Axial diameter (cm)	
Valleylab (formerly Radionics)	Cool-Tip RF 1-cm tip	Cooled	No data	No data	
Valleylab (formerly Radionics)	Cool-Tip RF 2-cm tip	Cooled	2.9 ± 0.3	No data	[111, 112, 114, 115]
Valleylab (formerly Radionics)	Cool-Tip RF 3-cm tip	Cooled	3.7 ± 0.6	No data	[111, 112, 114, 115]
Valleylab (formerly Radionics)	Cool-Tip RF cluster	Cooled	3.4 ± 0.4	4.0 ± 0.5	[114]
			3.6 ± 0.4	4.2 ± 0.6	[112]
RITA Medical Systems	Model 75/StarBurst	Expandable, multi-tined	2.0 ± 0.4	3.8 ± 1.4	[114]
RITA Medical Systems	Model 90/StarBurst XL	Expandable, multi-tined	1.5 (1.0–2.0)	4.9 (4.5–5.0)	[114]
			4.2 ± 0.2	4.3 ± 0.3	[112]
RITA Medical Systems	StarBurst MRI	Expandable, multi-tined	No data	No data	
RITA Medical Systems	StarBurst Flex	Expandable, multi-tined	No data	No data	
RITA Medical Systems	StarBurst Semi-Flex	Expandable, multi-tined	No data	No data	
RITA Medical Systems	Starburst SDE	Expandable, multi-tined	No data	No data	
RITA Medical Systems	Model 100/StarBurst XLi 50	Expandable-wet	No data	No data	
RITA Medical Systems	Model 100/StarBurst XLi 70	Expandable-wet	No data	No data	
Boston Scientific (Radiotherapeutics)	LeVeen 2-cm tip	Expandable, multi-tined	2.4 ± 0.3	2.0 ± 0.4 (1.2–2.7)	[114]
Boston Scientific (Radiotherapeutics)	LeVeen 3-cm tip	Expandable, multi-tined	No data	No data	[114]
Boston Scientific (Radiotherapeutics)	LeVeen 3.5-cm tip	Expandable, multi-tined	4.1 ± 0.3	3.5 ± 0.2	[114]
Boston Scientific (Radiotherapeutics)	LeVeen 4-cm tip	Expandable, multi-tined	4.3 ± 0.5	4.3 ± 0.4	[112]
Berchtold Medizinelektronik	HiTT 1-cm tip/1.2 mm diameter	Wet	No data	No data	
Berchtold Medizinelektronik	HiTT 1.5-cm tip/1.6 mm diameter	Wet	No data	No data	
Berchtold Medizinelektronik	HiTT 1.5-cm tip/1.7 mm diameter	Wet	No data	No data	
Berchtold Medizinelektronik	HiTT 1.5-cm tip/2 mm diameter	Wet	1.7 ± 0.4 (1.0–2.2)	3.0 ± 0.8 (1.8–4.2)	[114]
			3.4 ± 0.8	6.4 ± 1.9	[112]
Berchtold Medizinelektronik	HiTT 2-cm tip/1.6 mm diameter	Wet	No data	No data	
Berchtold Medizinelektronik	HiTT 2-cm tip/2 mm diameter	Wet	No data	No data	
Invatec	MIRAS IOC 3-cm tip	Cooled	No data	No data	
Invatec	MIRAS IOC 4-cm tip	Cooled	No data	No data	
Invatec	MIRAS IOC 5-cm tip	Cooled	No data	No data	
Invatec	MIRAS LC 2.5-cm tip	Cooled	No data	No data	
Invatec	MIRAS LC 3-cm tip	Cooled	No data	No data	
Invatec	MIRAS LC 3.5-cm tip	Cooled	No data	No data	
Invatec	MIRAS LN	Expandable, multi-tined	No data	No data	
Invatec	MIRAS RC	Expandable, spring	No data	No data	

convective cooling at the tip [23, 100]. Thermal conductivity of the tissue is improved by hydration; therefore, heat is carried away from the electrode quicker [97]. Hydration and increased ion concentration improve electrical conductivity of the tissue, even more so when using hypertonic saline [102]. This decreases resistive heating near the electrode and spreads the current density over a larger area [97]. Increased thermal and electrical conductivity cause a flattening of the temperature curve around the electrode, which permits greater energy

delivery to a larger area with less risk of tissue boiling, evaporation, and desiccation adjacent to the electrode [103, 104]. This risk of tissue boiling also is decreased by an increase in the boiling temperature of the saline-enriched tissue fluid [22, 27, 29, 34, 64, 99, 105]. When saline is infused at a low rate (1–2 mL/min) for a limited time (10 min), it remains concentrated in a small area (1–2 cm) around the electrode tip [106–108], forming a 'virtual' or 'liquid' electrode with a much larger diameter than that of the metal electrode. Because the diameter of RFA-induced coagulations is directly proportional to the electrode diameter [109]; accordingly, using a wet electrode can enlarge the thermal lesion [22, 34]. Of note, this liquid electrode can be irregular [108].

When higher infusion rates are used, contrast-stained saline has been shown to extend irregularly farther into the tissue and to leak along the electrode track [110]. This has led to unexpected damage to distant structures [111–113]. This kind of complication was more frequent for the wet electrode than for the cooled and expandable electrodes in comparative experimental studies [111, 112]. Although unproved, using small volumes of hypertonic saline might be preferable to larger volumes of isotonic saline [113].

An irregular shape to the thermal lesion with spread along vascular axes (type 2 deformity of RFA lesions according to Mulier et al [114]) has been noticed not only with high infusion speed [115] or large total volumes (>25 mL) [111] but also with low infusion rates and small volumes [22, 23]. This perivascular coagulation is worrying because in a comparative study of four commercial electrodes, the wet electrode killed five of eight animals compared with none for the other electrodes due to thrombosis of portal or hepatic veins [112].

A theoretical oncologic concern about wet electrode RF is that saline, which is contaminated with viable tumor cells, may leak out of the electrode track and cause peritoneal or track seeding. Another equally unproved concern is that the saline may increase the intratumoral pressure and force tumor cells into the circulation, thereby causing lymphatic and/or hematogenous seeding [22, 114].

Wet electrodes have been commercialized by Berchtold Medizinelektronik (Tuttlingen, Germany) as HiTT electrodes that have been described in detail elsewhere [114].

Cooled electrodes

The cooled electrode is an electrically insulated hollow electrode that contains a closed hollow channel [21, 33, 115]. The inner lumen is used to deliver saline or water to the tip of the electrode, and the outer lumen returns the fluid to a collection unit outside the body. The fluid does not leave the electrode. This way, the tip is internally cooled to a temperature lower than 25°C to prevent charring of the tissue immediately adjacent to the tip [33]. A recent study has indicated no significant effects of coolant temperature on hepatic RFA lesion size induced by this electrode [116].

A theoretical inconvenience of this method is that the tumor immediately adjacent to the electrode is spared during the coagulation. However, after stopping the coagulation and the perfusion, heat diffuses from the peripheral to the central part of the thermal lesion so that the central cells are probably killed too [21]. When the electrode is pulled out immediately, there is a danger of seeding viable central cells into the track [13]. To prevent this, the electrode track should be cauterized on withdrawal.

The cooled electrode has been commercialized by Radionics (Ghent, Belgium) and more recently by Invatec (Roncadelle, Italy) [114]. The Radionics Cool-Tip single electrode has a sensor at the tip to allow for continuous temperature and impedance measurement. Because it is straight, the Cool-Tip is the sole electrode until now that can be used for RF-assisted hepatic resection, in which the future plane of transsection is coagulated before transsection [117]. The Invatec MIRAS LC and IOC flexible electrodes have a bent thermistor that curves away from the tip to monitor tissue temperature.

In the Cool-Tip Cluster electrode (Radionics) [118], three parallel cooled electrodes are mounted on the same shaft at a distance of 5 mm. The electrodes are activated simultaneously. The larger contact surface allows higher current intensities with less possible charring around the tip and therefore larger thermal lesions than in single cooled electrodes [118, 119]. A disadvantage of the cluster electrode is that it is more difficult to insert percutaneously through a narrow intercostal space or by a very oblique subcostal approach than the single cooled electrode [120]. Further, it is harder to visualize all three electrodes at the same time, so that inadvertent injury to structures, e.g., blood vessels, is more likely.

Expandable electrodes

An expandable electrode is inserted as a straight insulated needle into the tissue. Once in the desired position, the active electrode is deployed from the hollow shaft of the probe. Two types exist: the multi-tined type and the spring type.

Multi-tined expandable electrodes [121] compose an array of four to 12 curved electrode tines (prongs) that are deployed from the hollow needle tip. The electric field follows the configuration of the deployed prongs. The larger contact surface between electrodes and the tissue decreases the chance of charring. Due to the Faraday cage effect, coagulation starts at the extremities of each prong and then forms coagulation tubes around each prong, which subsequently fuse, first centrally and then at the periphery, to form a more or less spherical coag-

ulation zone [122–126]. In perfused liver, fusion between the individual coagulation tubes around each tine is not always complete and may show clefts, resembling a cloverleaf or a daisy [114]. In the first years that expandable electrodes were used, the RF generator was started only after complete deployment of prongs. More recently, it has been shown that RFA with gradual expansion in two or more steps yields larger coagulation zones. When prongs are deployed only partly, current is concentrated in a smaller area, leading to more reproducible complete heating of this zone. By then fully extending the prongs, a larger and more complete lesion is achieved [127, 128]. This stepwise expansion is now incorporated in the protocols of the newest RITA electrode.

Multi-tined expandable electrodes have been commercialized by three companies. RITA Medical Systems (Mountain View, CA, USA) has Christmas tree-like electrodes with temperature sensors at the tip of each prong [129]. The shaft is straight or flexible. The Boston Scientific (Natick, MA, USA; formerly Radiotherapeutics) electrodes have an umbrella shape [122]. The prongs of the more recent Invatec electrodes are curved in the opposite way and are deployed by pulling rather than by pushing [114].

Expandable spring electrode

The MIRAS RC is a unique type of electrode with a coil that leaves the tip and is deployed perpendicularly to the shaft [114].

Expandable-wet electrodes

Miao et al. and Rhim et al. independently described the expandable-wet electrode, which combines features of both techniques and which is more effective than the wet or expandable electrode separately [29, 130–134]. Ex vivo, lesions up to 10 cm [29] have been obtained with this method. Lesions are roughly spherical but often show irregular extensions along blood vessels [29]. Unexpected hepatic and perihepatic burns were noted with high-speed saline infusion [110]. The expandable-wet electrode has been commercialized by RITA as the model 100/StarBurst XLi electrode [110, 114].

Experimental electrodes and saline-enhanced RFA

Many more electrodes are in the preclinical experimental phase, such as the cooled-wet electrode that allows continuous infusion of interstitial hypertonic saline around the tip of a cooled electrode. The cooled-wet electrode produces larger coagulation zones than the wet or the cooled electrode does separately [27, 108, 135–138]. Potential for tumor eradication has been shown in patients who had HCCs as exemplified here by a clinical

case, of which coagulation diameters more than 7 cm could be obtained by activation of the prototype cooled-wet electrode in one RFA session (Fig. 2).

In saline-enhanced RFA [82, 104, 105, 108, 139], saline is injected into the tissue as a bolus before RFA, and the injection needle is not incorporated into the electrode (in contrast to the wet or the cooled-wet electrode) and, therefore, should not be confused with the "wet-electrode". A full description of experimental electrodes [27, 29–31, 108, 140] and saline-enhanced RFA is beyond the scope of this report. Despite early disappointing conclusions about instilling saline during RFA and using hypertonic saline [82], these approaches (alone or combined) have been further applied and refined [22, 27, 29, 34, 64, 97–108, 110–113, 118, 131–133, 135–141]. However, in the approach of saline injection before RFA, as with intramuscular injection of a solution, the saline is diffused or absorbed rapidly not only in but also beyond the target tissue, especially in well-perfused organs. Therefore, the proportion of injected saline required to enhance RFA efficacy and the potential for the aforementioned adverse effects remain uncertain and uncontrollable. That is the reason a minimum preinjection coupled with slow simultaneous infusion of hypertonic saline during RFA has been regarded as an indispensable element for improved ablation efficacy [22, 27, 29, 34, 64, 99, 131–133, 135–138]. Interestingly, one recent in vivo animal study concluded that hypertonic saline instillation before RFA is better than simultaneous instillation during RFA [142], which seems partly in line with one previous report [82] but contradictory to most others [22, 27, 29, 34, 64, 99, 131–133, 135–138] and, hence, needs to be further verified.

Commercial RF generators: design and working principles

The five companies that produce commercially available electrodes each have their own generators that are compatible only with their own electrodes. The specifications of the generators are presented in Table 3.

Valleylab (formerly Radionics)

The Radionics system consists of a generator and a perfusion system. Maximal power is delivered during a predetermined period (usually 12 or 15 min) [114]. Needle cooling is ensured by internal perfusion of chilled saline and is started 1 min before the start of RF coagulation. If impedance increases to 10 Ω above the baseline value, power is automatically switched off for 15 s and then switched on again [112]. This automatic control mode yields larger lesions than does continuous power output, but it has been somehow misleadingly called "pulsed" RFA since it was initially introduced [26]. What is important is not the *pulse* but the *pause*,
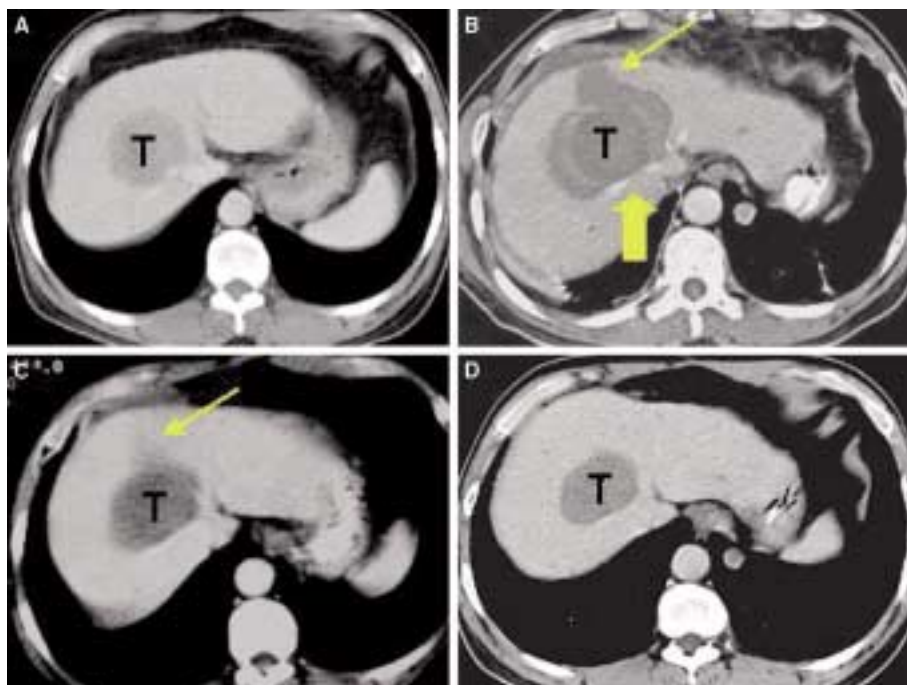
Fig. 2. A clinical example of using a prototype cooled-wet electrode. Contrast-enhanced CT scans before (A) 2 weeks, (B) 3 months, (C) and 9 months (D) after cooled-wet electrode mediated RFA in a patient with a 5-cm HCC located in the right liver lobe. The RFA was conducted under laparotomy by a single electrode insertion with a Pringle maneuver for 18 min, power output at 150 watts and 10% saline infusion at 1 mL/min after preinfusion for one minute. Notice that the coagulation diameter over 7 cm involves both the entire tumor (T) and an over 1 cm broad oncological margin except where the tumor borders the right hepatic vein (thick arrow). The thin arrow indicates the burned electrode track (B), which was gradually healed (C, D). At 18 months follow-up, the patient is still free of tumor with his serum alfa-fetoprotein decreasing from over 800 ng/mL before RFA to below 3 ng/mL after RFA and still remaining normal, suggesting possible tumor eradication.

Table 3. Specifications of commercial radiofrequency ablation generators

	Valleylab (Radionics)	RITA Medical Systems	Boston Scientific (Radiotherapeutics)	Berchtold Medizinelektronik	Invatec
Name of generator	CC-1 Cosman coagulator	RITA 1500X RF generator	RF 3000 generator	Elektrotom HiTT 106	TAG 100 W
Frequency (kHz)	480	460	460	375	460
Maximal power (W)	200	250	200	60	100
Power mode	Continuous or pulsed	Continuous	Continuous	Continuous or pulsed	Continuous
Power monitoring	Yes	Yes	Yes	Yes	Yes
Current monitoring (A)	0–2.0	No	No	No	No
Impedance monitoring (Ω)	Yes	Yes	Yes	Semiquantitative	Yes
Temperature (°C) monitoring of n channels	1	9	0	1	4
Automatic power control	Yes, impedance based	Yes, temperature based	No (hand control)	Yes, impedance based or temperature based	No (hand control)
Approved by European Community	Yes	Yes	Yes	Yes	Yes
Approved by U.S. Food and Drug Administration	Yes	Yes	Yes	Yes	No

Table 4. Comparison between thermal coagulation necrosis and (classic) coagulation necrosis

Features	Thermal coagulation necrosis	(Classic) coagulation necrosis
Causes	Physical (RFA, ILT, MWA, etc.)	Biological (ischemia, trauma, infection, etc.)
Occurring time	Seconds to minutes	Hours to days
Effects	Tissue fixation	Enzymatic cytolysis
Macroscopic aspects	~3–5 Zones	Zoneless, amorphous
Microscopy (HE staining)	Almost intact in tissue architecture and cell composition (middle zone)	Cytoplasmic eosinophilia, nuclear karyorrhexis and remnant tissue architecture
Microscopy (enzymatic histochemical staining)	Negative	Negative
Immunohistochemical assays	Maybe weakly positive	Negative
Duration before repaired	Up to months	Up to weeks

HE, hematoxylin and eosin; ILT, interstitial laser thermotherapy; MWA, microwave ablation; RFA, radiofrequency ablation

i.e., the timely interruption of current when impedance starts to increase, which allows the dissipation of gaseous buildup between electrode and tissue. Without pause, such evaporated gas can insulate part of the electrode tip, and the entire current will be loaded on the rest of the tip, rapidly resulting in charring, increased impedance, and cessation of the RF generator. The presence of a strict rhythm or regular intervals governs whether or not the term *pulsed* should apply. The real pulsed RFA does exist but has not been applied for tumor ablation [143, 144].

RITA

The RITA generator is used as such for the expandable StarBurst XL electrode and in combination with a perfusion system for the expandable-wet StarBurst XLi electrode. Tissue temperature is measured at the tip of the prongs. There are two possible ways to use the generator [145]. In the first, a target temperature is chosen, and power is adjusted automatically to reach and hold this temperature (temperature control mode) [146]. Alternatively, power can be fixed at a chosen level until a desired temperature is reached (power control mode) [112]. In both methods, only temperature and not impedance is taken into account, in contrast to other generators. The electrode is deployed gradually according to treatment algorithms described elsewhere [112, 114]

Boston Scientific (Radiotherapeutics)

For the Boston Scientific (Radiotherapeutics) RF 3000 generator, power output is set manually. Treatment algorithms are based on a stepwise power increase during fixed periods [114]. Neither temperature nor impedance is taken into account. Treatment is continued until power is shut off by a sudden increase in impedance. A short pause allows dissipation of gas between electrode and tissue, after which a second cycle at a lower power level is

started. Although this pause has the same aim as the pauses in the pulsed modes for the Radionics and the Berchtold generators, the Boston Scientific (Radiotherapeutics) generator has to be restarted manually. Treatment is stopped when the second power shutoff occurs.

Berchtold

The Berchtold system consists of a generator and a perfusion system. The power level and the duration are chosen according to a treatment algorithm [114]. This power level is further adjusted by one of two automatic power control modes: impedance control or temperature control [147]. If impedance becomes too high in the impedance control mode, power is interrupted automatically for a few seconds until impedance returns to normal values, in a way similar to the pulsed mode for the Radionics system. Similarly, in the temperature control mode, power is shut off temporarily if a predetermined temperature threshold is reached. Perfusion is started 1 min before staring RF energy delivery. Perfusion speed is controlled automatically based on power and tissue impedance [112]. When impedance becomes too high, an extra bolus of saline is injected to disperse any gaseous buildup around the electrode [112].

Invatec

For the Invatec TAG 100 W generator, power output is set manually. Treatment algorithms are based partly on a stepwise power increase during fixed periods and partly on tissue temperature feedback from the thermistor that bends away from the tip of the electrode [114].

Size and geometry of hepatic RFA lesions

In RFA of liver tumors, precise tailoring of the size and shape of the thermal lesion is important. The coagulated
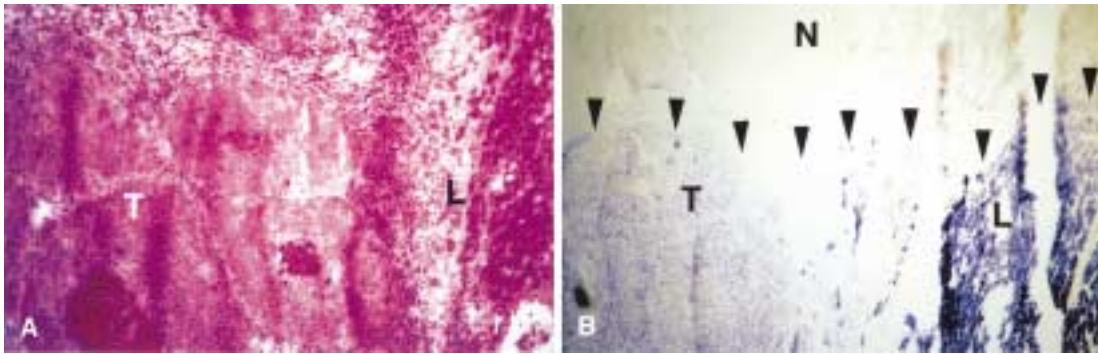
Fig. 3. Serial frozen sections and photomicrographs with (A) HE staining and (B) nicotinamide adenine dinucleotide histochemical staining of the VX2 tumor-bearing liver from a rabbit immediately after incomplete tumor RFA. Although the differences between ablated and unablated tumor (T) and normal liver (L) can not be readily seen with HE staining due to the so-called thermal fixation or ghost effect (a), the margins (arrowheads) of the ablation are sharply circumscribed with nicotinamide adenine dinucleotide staining (b). In comparison with negative staining in the RF-ablated tumor and liver tissues (N), oxidative enzymatic activity appears much stronger (+++) in normal liver (L) than that (+) in viable tumor (T). Original magnification 100×.

area should be large enough to encompass the tumor and a safety margin of 1 cm at all sides. Because US monitoring of the coagulation zone is unreliable, exact prior knowledge of the size and shape of a single-session RFA lesion and its relation to the electrode tip is essential [114].

Size and geometry of hepatic RFA lesions by commercial electrodes have been analyzed in a recent exhaustive review [114]. The paucity of available data is striking. Many descriptions of RFA lesions are limited to the mean transverse diameter. Data on length (axial diameter), distortion, completeness, and spatial relation to the electrode tip are rare to nonexistent. As of January 2004, data on the most basic parameter (transverse diameter) in the perfused pig liver are available for only nine of the 30 electrodes that are presently on the market (Table 2). Values for the same parameter using a Pringle maneuver are available for only one of the 30 electrodes.

With normal blood flow, diameter and length of RFA lesions in pig liver are often smaller and more variable than the length of the electrode tip or the diameter of the deployed prongs suggests [114]. RFA lesions are not always perfectly spherical. They often resemble ellipses or flattened spheres [114]. In the perfused liver, a type 1 distortion of the RF lesion (a lesion asymmetrically smaller than expected) by the heat-sink effect of nearby blood vessels is very common for all electrodes [114]. This distortion frequently causes incomplete ablation and local recurrence. A type 2 distortion (a lesion irregularly larger than expected) is seen mainly with the wet electrode and saline-enhanced RFA and can cause unwanted damage [114]. Surgical clips near the tumor are another source of type 2 distortion [148]. Incomplete fusion of RFA lesions between prongs is noted for RITA and Radiotherapeutics expandable electrodes [114].

Compared with RFA in perfused liver, thermal diameter is larger when performing RFA during partial or total blood flow interruption in pig liver and in patients who have liver tumors [114]. Distortion is less frequent and complete fusion is more frequent with hepatic vessel occlusion [114]. All these findings are more pronounced in cases of complete interruption of inflow (Pringle maneuver) or outflow (occlusion of hepatic veins) as compared with partial occlusion, i.e., only the hepatic artery or the portal vein [114, 149]. This may partly explain the trend toward less local recurrence (4–9%) in series using a Pringle maneuver rather than a percutaneous approach alone (30–60%) [114].

Pathophysiologic process of thermal coagulation necrosis

The pathogenic conditions posed by RFA fundamentally differ from those of ordinary tissue death and cannot be readily recognized without a lot of experience or interpreted using classic medical knowledge [34]. Even skilled pathologists may fail to correctly diagnose a typical RFA lesion under routinely processed microscopy, especially only at needle biopsy, without an overview of the entire cross-section. Therefore, to identify this unique type of heat-related tissue pathology, it is necessary to understand the essential differences in mechanisms of action between commonly occurring and RFA-induced tissue death (Table 4).

Necrosis, by classic definition, means pathologic cellular or tissue death in a living organism, irrespective of the cause and is the sum of the morphologic changes indicative of cell death caused by the progressive degradative action of enzymes; it may affect groups of cells or part of a structure or an organ. When normal cells are

Table 5. Histomorphologic features of radiofrequency ablated lesions

Zone	Macroscopy	Microscopy (hematoxylin and eosin)
A	Needle track	Microcavitation and/or charred area
B	Ablated tumor	Intact tumor tissue architecture (thermal fixation)
C	Ablated peritumoral tissue	Intact normal tissue architecture (thermal fixation)
D	Dark rim	Hemorrhage with typical necrosis
E	Vague outer band	Hyperemia, inflammatory infiltration, edema

Table 6. Histopathologic comparison of tissues without and with RFA

Tissues without and with RFA	Nuclear and cytosolic staining (HE)	Enzymatic staining (e.g., NADH or TTC)
Normal tissue[a]	Present	Positive (+ + +)
Tumor tissue[b]	Present	Positive (+ ∼ + +)
Normal tissue with RFA[c]	Present	Negative
Tumor tissue with RFA[c]	Present	Negative
Tumor-native necrosis	Absent or poor	Negative

[a]Outside the RFA lesion
[b]Spared fiom RFA (incomplete ablation)
[c]Middle zone
HE, hematoxylin and eosin; NADH, nicotinamide adenine dinucleotide-diaphorase; RFA, radiofrequency ablation; TTC, 2,3,5-triphenyl-tetrazolium chloride

lethally injured in common conditions (ischemia, trauma, infection, etc.), the resultant membrane dysfunction and subsequent internal release of various enzymes eventually proceed to degrade cellular structures and constituents. This is the classic process of necrosis; unfortunately, current morphologic means are not sensitive enough to detect its initial point. These enzymatic reactions result in a number of microscopically observable changes, e.g., nuclear karyorrhexis due to membrane and chromatin fragmentation into irregular pieces and cytoplasmic eosinophilia due to enzymatic degradation of cytosolic RNA and proteins. These changes are characteristic of a typical coagulation (or coagulative) necrosis, i.e., remnant tissue architecture with ruined cellular composition. The entire process takes hours to days followed by a few weeks of tissue repairing. Intratumoral spontaneous necrosis may also belong to this category, although it appears more amorphous without obvious healing signs.

In contrast, the moderately elevated temperature of 50°C to 100°C during RFA produces an area of immediate tissue coagulation. This constitutes the major portion of the RFA lesion and occupies the area between the immediate perielectrode zone and the periphery of the lesion. The affected life structures and substances including cytosolic enzyme proteins in particular are subjected to an instantaneous thermal fixation, an effect equivalent to that with formalin used for routine histopathology. Because of such thermally induced structural denaturalization and functional deactivation of the enzyme proteins, all the aforementioned progressive enzymatic tissue or cell degradation as seen in the process of traditionally defined coagulation necrosis becomes impossible. As a consequence, with conventional staining techniques, the tissue architecture and cytologic details appear well preserved, despite an absence of any activity on enzymatic histochemical assays (Figs. 1c, 3) [34, 120, 125, 149, 150]. This has been described in the literature as the ghost phenomenon or thermal fixation [34, 64, 65, 67, 69, 151, 152]. However, the loss of enzymatic activity does not exclude antigenicity of the denatured enzyme proteins that have undergone thermal (RFA) or chemical (formalin) fixation, which explains certain positivity in

RFA lesions of thermal coagulation necrosis with immunohistochemical examinations [99]. In other words, immunoassays can be less reliable than enzymatic staining for tissue viability determination. The pronounced effects of vascular destruction with RFA often postpone the healing of the ablated region by blocking neutrophils with hydrolytic enzymes from access into the lesion, frequently resulting in incomplete absorption and fibrous encapsulation of the residual lesion [34, 64, 65, 67, 69, 152]. Gradual fading of cytologic staining properties with hematoxylin and eosin (HE) dyes and evolving classic coagulation necrosis may take as long as many months [34, 64, 65, 67, 69, 150, 152], although one clinical study reported this finding as soon as 3 days [120], which contradicts another clinical study that also included observations at 3 days [150]. Aside from such representative alterations in the median zone of a RFA lesion, the excessive heat around the needle track often causes tissue microcavitation and carbonization in the central zone, whereas the mild heat in the outer zones stimulates tissue reaction, resulting in cell injury and even typical necrosis due to released enzymes from the infiltrating neutrophils.

To avoid confusing terminology as has appeared in the literature [19, 21, 26, 79, 125, 149, 153], to make a clear distinction in the future documentation, and to make the minimum necessary changes, it seems logical to stipulate the nomenclature of these two totally different sets of necrosis as *(classic) coagulation necrosis* and *thermal coagulation necrosis* (Table 4), whereas *thermal fixation* sounds more like a technical process than a pathologic status [152].

Morphologic features of RFA-induced lesions

Extensive histopathologic investigations on excised and biopsied specimens obtained from experimental animal research and clinical patient studies on various thermo-

therapies for malignant tumors have not only enriched our conceptual understanding of this unique type of pathology but also built up our experience in correctly interpreting the manifestations of RFA lesions at different stages [34, 64, 65, 67, 69, 99, 120, 125, 149–152]. In practice, it appears easier to identify a RFA lesion by gross inspection than by microscopic observation (Table 5).

Macroscopically on cross-sections, a typical lesion of RFA tumor eradication appears well demarcated and contains the following five zones that reflect degrees of tissue damage along the temperature gradient outward: zone A, the dark overheated carbonized or vaporized center surrounding the needle track; zones B and C, the pale or tan moderately heated broad zones of coagulated tumoral and peritumoral tissue, respectively; zone D, the distinct reddish (fresh) or brown (formalin-fixed) mildly heated hemorrhagic rim; and zone E, the faint outer layer of hyperemia and/or edema [34, 65, 67] (Table 5). The presence or absence of the peripheral two layers distinguishes between in vivo and ex vivo RFA lesions [27, 34]. Mitochondrial enzymatic histochemical staining with 2,3,5-triphenyltetrazolium chloride can be used to distinguish dead from viable tissues on the surface of tissue sections but may confound native tumor spontaneous necrosis and RFA-induced tissue coagulation [120, 153–158] (Table 6). The global shape of the RFA lesion is not necessarily spherical and can be altered by factors such as perfused blood vessels passing through or by the ablative region, as discussed elsewhere [34, 111, 114, 149, 152].

Microscopically, the center (zone A) and the two outer layers (zones D and E) of a typical RFA lesion can be easily recognized according to the corresponding characteristic changes in tissue structure and cell compositions. It is the in-between coagulated zone, which forms the dominant part of the lesion and includes tumoral (zone B) and normal (zone C) tissues, that appears most tricky to identify with routine histopathologic assessment, especially soon after therapy, because the RFA-treated tissues in this region do not meet the classic criteria for having undergone typical coagulative necrosis [34, 64, 65, 67, 69, 99, 150–152]. Instead, having been thermally coagulated or fixed, tumoral and normal cells and tissues in this zone look almost identical to those without RFA at HE-stained microscopy (Fig. 1b vs. 1c, Tables 5, 6). Therefore, for therapeutic confirmation, especially by fine-needle aspiration, this technique may cause false-positive results that show cytologically "viable" cells that have actually been devitalized and will sooner or later undergo coagulative necrosis [150, 159]. It is also less sensitive to residual viable tumor immediately after RFA than at the follow-up weeks or months later, when the cytologic staining properties with HE dyes gradually fade out and the classic coagulative necrosis appears [34, 64, 65, 67, 69, 150–152].

Nonetheless, cell viability in the ablated zone soon after RFA can be absolutely determined by a negative reaction with the enzymatic histochemical stains such as lactate-dehydrogenase, maleate-dehydrogenase, or nicotinamide adenine dinucleotide-diaphorase [34, 120, 125, 149, 150]. Only recently has this technique become the accepted gold standard for tissue viability determination after RFA at the cellular level [34, 120, 125, 149, 150], despite the fact that its importance had long been demonstrated with other thermal ablation techniques [151, 160]. The enzymatic techniques may also help to differentiate cellular types by demonstrating degrees of staining between normal and malignant and between viable and dead cells (Fig. 2a,b, Table 6). However, a combined use of HE and enzymatic stainings from serial frozen sections is recommended for better analysis of viability and morphology [34, 126]. Nevertheless, a careful inspection of the different zones on an HE-stained cross-section, especially under a low magnification microscope, may allow the correct diagnosis of an RFA lesion [34, 64, 65, 67, 69, 152] after taking the following features into account: (a) a well demarcated lesion, (b) gradient damage in five zones, and (c) vascular thrombosis with air bubbles (Fig. 1a–c).

In reality, these zonal features can vary in intensity and extent in each zone for a given RFA lesion depending on the causative temperatures. For instance, zone A with severe tissue desiccation can be predominant in relatively small lesions induced by intense RF current delivery through dry electrodes, and then the typical thermal coagulation (zones B and C) can become less obvious [126]. With advanced technologies for creating larger RFA lesions at more adequate RF energy delivery, like cooking a medium-done (but not over- or well-done) steak, it should not be surprising to see the thermal fixation or ghost phenomena more frequently [34, 64, 65, 67, 69, 151, 152]. In contrast, if insufficient RF current is applied, the "rare-done" lesions may contain severely injured cells with activated cytosolic enzymes and/or undestroyed blood vessels bringing in neutrophils; both jointly create typical enzymatic tissue damage. This could be one of the possible explanations for the reported uncommon real coagulative necrosis 3 days after RFA [120].

As for whether there are RFA-specific histopathologic features, in 1924, Clark et al. published a classic description of electrocoagulation in the desiccation (i.e., "over- or well-done") mode of RF current [161]. They described certain characteristic changes including shrunken and shriveled cells with condensed and elongated nuclei that produced a "mummified" appearance [161]. This is almost identical to the desiccation change seen in the RFA lesion in patients treated with a modern dry electrode [126]. Another recent clinical report displayed a photomicrograph of "abnormal elongated tumor cells with dense spindle-form nuclei and streaming cytoplasm." This was regarded as a common finding after RFA as a result of heat preservation or electrocautery effect [120]. Despite the lack of wide support
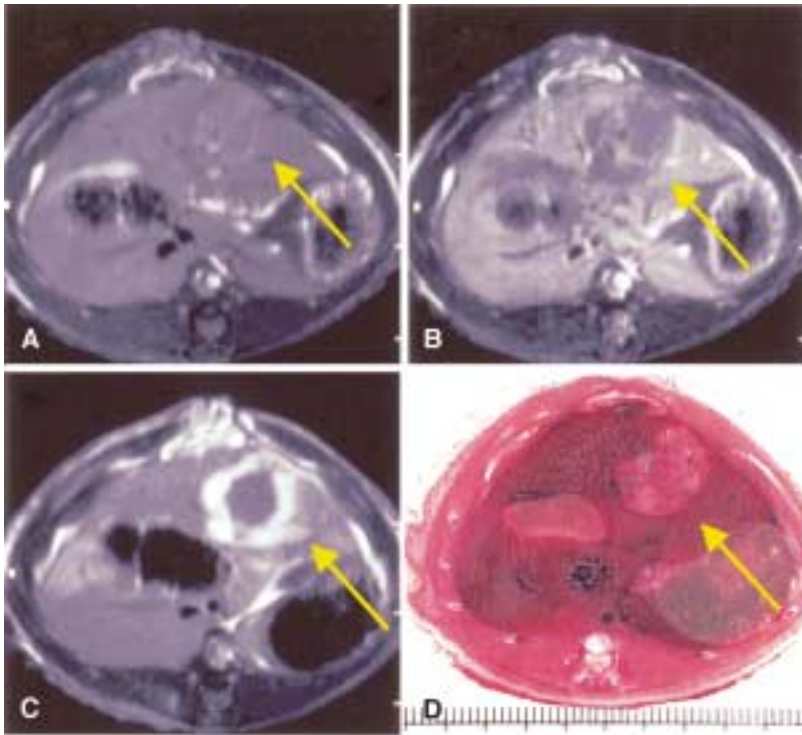
Fig. 4. (A–C) T1-weighted MR images and (D) corresponding cross-section from a rat-bearing liver implanted rhabdomyosarcoma 1 day after cooled electrode-mediated RFA. Although virtually indiscernible before contrast (A), 5 min after intravenous injection of a non-porphyrin NACA, the RFA lesion (arrow) is demarcated as a hypointense area relative to the strongly enhanced liver (B). A few hours after NACA injection, the lesion has striking rim enhancement encompassing the ablated tumor and marginal liver tissue (C), which persists for a few days and matches well with the histomorphologic section (D), indicating complete tumor ablation.

from the literature [34, 62, 63, 65, 67, 151, 152, 159], similar histologic descriptions have been adopted in a series of subsequent laboratory studies in rats with an experimental breast tumor [154, 156, 157]. However, the demonstrated histologic findings did not convincingly match the described changes characteristic of RFA [154, 156, 157]. Therefore, whether this notion represents the real truth needs to be verified by future clinical and animal research. Morphologically, the potential pitfalls could be (a) mistaking ablated dead tissue for viable tissue at conventional microscopy [99, 150], (b) mistaking intratumoral spontaneous necrosis for RFA-resultant coagulation necrosis [63, 120, 153–159], and (c) rendering certain nonspecific histologic findings as characteristic for RFA. Further, there have been found a few false technical descriptions in previous RFA studies such as the erroneous use of the macroscopic histochemical staining agent 2,3,5-triphenyltetrazolium chloride to fix tumor tissues for light microscopy [120, 153] and the confused nomenclature between oxidative enzymatic and immunohistochemical stainings [111, 120].

Applications of imaging modalities in RFA

Imaging technology has played an important role in the diagnosis, treatment planning, guidance of percutaneous, laparoscopic, or intraoperative electrode positioning, real-time monitoring of the RFA procedure, and postprocedural evaluation of the therapeutic response [162–167].

Although US has been most widely used for guiding the placement of RFA electrodes, good real-time US monitoring of all margins of RFA lesions appears difficult or impossible because of the presence of microbubbles from vaporization of intracellular water during RFA [111], as shown by basic research [168]. In contrast, unenhanced CT has been promoted as an effective way to monitor RFA compared with US because of improved lesion discrimination, reproducible decreased attenuation during ablation, and better correlation to pathologic size [169]. MRI may offer further advantages over US and CT for guiding and monitoring RFA procedures provided a fully magnetically compatible RFA system and a swift and interactive MRI-RFA alternating system become available at reasonable costs [170, 171].

Assessment of RFA therapeutic responses with imaging modalities represents another challenge. Nonspecific findings with plain scans such as altered regional echogenicity on US, densities on CT, or signal intensities on MRI have been found inaccurate and unreliable for the extent of induced coagulation. With the use of commercial contrast agents, CT and MRI demonstrate circumscribed hypodense or nonenhancing regions surrounding the electrode tract as soon as a few minutes after RFA, thus reflecting the extent of tissue destruction. The most accurate predictor of induced coagulation is believed to be the identification of a previously enhancing tumor but void contrast enhancement after RFA (Fig. 2). Nevertheless, two key limitations of current techniques remain: insufficient spatial resolution for detecting small residual foci of
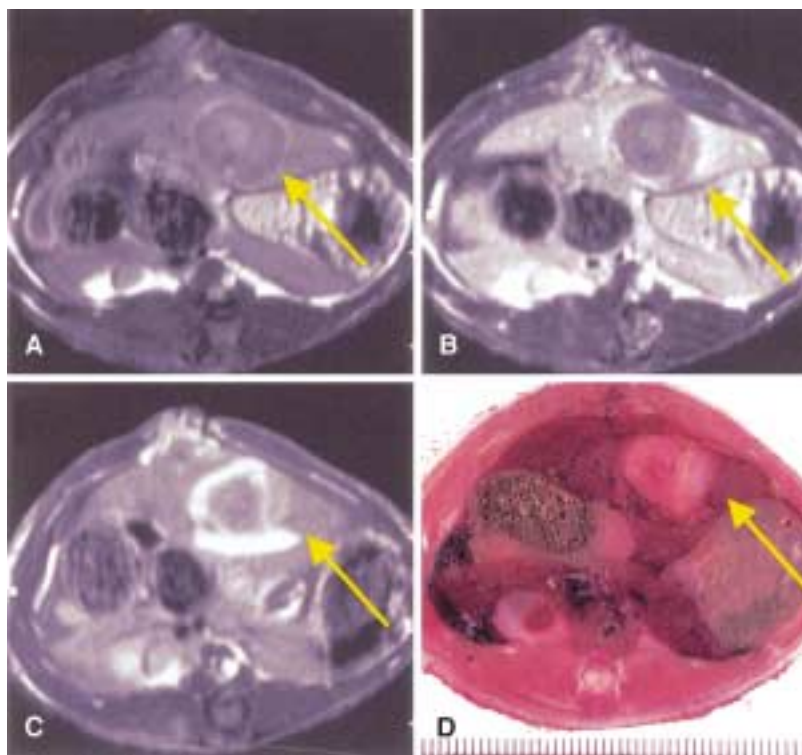
Fig. 5. (A–C) T1-weighted MR images and (D) corresponding cross-section from a rat-bearing rhabdomyosarcoma in the liver 1 day after an intended, incomplete RFA. Although just discernible before contrast (A), 5 min after intravenous injection of NACA, the RFA lesion (arrow) is demarcated as a hypointense area relative to strongly enhanced liver (B). The viable tumor also enhances, but to a much lesser degree, in comparison with normal liver at this early stage. One day after NACA, the characteristic contrast due to its specific effect enables differentiation between ablated tumor and marginal liver tissue and between viable residual tumor and normal liver (C), as proved by histomorphologic section (D), which shows the effect of an in vivo "histochemical staining" MRI technique.

peripheral tumor (the likely cause of later "recurrence") and inadequate imaging specificity for the differentiation between tissue inflammatory reaction and incompletely ablated viable tumor after RFA procedure. Therefore, current ablation strategies attempt to destroy a peripheral 1-cm rim of apparently normal tissue surrounding the tumor margins to ensure complete local disease control, although this is not always possible. Thus, periodic imaging follow-up every 3 to 6 months has become common clinical practice to enable the detection and further treatment of residual tumor after interval growth [24, 172]. By comparing pulse inversion contrast-enhanced harmonic US, contrast-enhanced power Doppler US, and helical CT in a clinical setting, Meloni et al. concluded that contrast-enhanced pulse inversion harmonic imaging may enable the detection of residual nonablated tumor in more cases than contrast-enhanced power Doppler US and may ultimately prove to be a useful adjunct for percutaneous ablation therapies, but admitted that contrast-enhanced axial CT and MRI are still the most sensitive tests for managing thermal ablation in patients who have HCC [173]. However, in line with previous animal studies [174], Choi et al. clinically demonstrated equivalent efficacy between contrast-enhanced gray-scale harmonic US and contrast-enhanced CT for the early assessment of therapeutic response of HCC to RFA [175]. New techniques are still emerging; for example, sonographically based elastography was found reliable for delineating thermal lesions resulting from RFA [176].

Thus far, the visual effects created with all currently applied in vivo imaging techniques on RFA-induced lesions are nonspecific, indirect, and inaccurate in a sense that it is impossible to make a clear-cut distinction between the ablated dead tissues and unablated viable tissues that might be injured but still vital [177], as seen with ex vivo enzymatic staining. However, the recent discovery and refinement of a new type of specific imaging markers, namely necrosis-avid contrast agents (NACAs), may provide a virtual in vivo surrogate of "histochemical staining" for noninvasive imaging determination of tissue viability [178–181]. These agents firmly label nonviable tissues and are seen as persistent strong contrast enhancement or hotspots on MRI or nuclear imaging independent of tissue origin or the cause of necrosis [182–186]. Equal to the potential utility in myocardial viability determination [187–191], the other promising application of NACAs is the postprocedural assessment of minimally invasive ablation therapies including RFA [192, 193]. NACA-mediated imaging modalities could help to identify complete or incomplete treatment so that the therapeutic regime can be adjusted in a timely fashion, i.e., during the same hospital admission but not the same treatment session. Soon after systemic administration of NACA, the ablated lesion appears as a nonenhancing region relative to enhanced normal tissue. On delayed imaging after several hours, the characteristic striking contrast enhancement depicts exactly the lesion of thermal coagulation necrosis in contrast to unablated normal tissue and incompletely

ablated viable tumor tissue as proved by histomorphology (Figs. 4, 5).

Conclusion

RFA represents a local devitalizing therapy of an old principle but with newly upgraded applicability due to advances in technology. As a result of massive experimental and clinical research over the past decade, it has rapidly evolved into a major player in the armamentarium of minimally invasive cancer therapies. Since the first reports on hepatic RFA, many electrodes have been commercialized and new models are expected to emerge in the market. The same electrode and treatment algorithms may yield coagulation lesions with a wide range of volumes, resulting in varying reports from different groups. Many coagulation lesions are incomplete or distorted, especially with normal blood flow. This nonideal reality calls for research focused on the development of electrodes and methods that yield coagulations with more reliable diameters and are less susceptible to the heat-sink effect. RFA results in "thermal fixation" of the tumor and a normal margin due to a sudden deposition of a lethal temperature. This mechanism of injury has unique features that distinguish it from classic coagulative necrosis. Understanding of the underlying pathophysiologic process may facilitate identification and explain the histomorphologic appearance of the RFA lesions at different stages. Aside from further improving guidance and monitoring of the RFA procedure, the development of an in vivo "virtual histochemical staining" technique for noninvasive assessment of RFA therapy by imaging modalities may prove crucial for an optimized treatment protocol. Although research until now has focused on ever larger lesions, there are now additional priorities including increased reliability, more tailored ablation, more accurate data generation, and standardization of documentation and communication.

References

1. Organ LW (1976) Electrophysiologic principles of radiofrequency lesion making. Appl Neurophysiol 39:69–79
2. Hand WJ, ter Haar G (1981) Heating techniques in hyperthermia. Br J Radiol 54:443–466
3. Freund F (1908) Die elektrische funkenbehandlung (fulguration) der karzinnome vol. 2 Stuttgart: Ferdinand Enke
4. Keating-Hart W (1909) La fulguration et ses résultats dans traitement du cancer d'après une statistique personelle des 247 cas. J Med Intern (Paris) 13:41–50
5. Doyen E (1910) Traitement local des cancer accessibles par l'action de la chaleur au-dessus de 55°C. Rev Ther Med Chir 77:551–557
6. Clark W (1911) Oscillatory desiccation in the treatment of accessible malignant growths and minor surgical conditions. J Adv Ther 29:169–183
7. Strauss AA, Strauss SF, Crawford RA (1935) Surgical diathermy of carcinoma of the rectum. Its clinical end results. JAMA 104:1480–1484
8. Sheski FD, Mathur PN (1999) Cryotherapy, electrocautery, and brachytherapy. Clin Chest Med 20:123–138
9. Cushing H (1928) Electro-surgery as an aid to the removal of intracranial tumors. Surg Gynecol Obstet 47:751–784
10. Geddes L, Silva L, Dewitt D (1977) What's new in electrosurgical instrumentation? Med Instrument 11:355–359
11. Memon MA (1994) Surgical diathermy. Br J Hosp Med 52:403–407
12. Massey GB (1925) Lectures, clinicals and discussions on electrophysiotherapy, vol 73 Chicago: Fischer
13. Mulier S, Mulier P, Ni Y, et al. (2002) Complications of radiofrequency coagulation (RFC) of the liver tumors: rate, causes, prevention and treatment. Br J Surg 89:1206–1222
14. Pawl R (1975) Percutaneous radiofrequency electrocoagulation in the control of chronic pain. Surg Clin North Am 55:167–179
15. Huang SK, Bharati S, Graham AR, Lev M, Marcus FI, Odell RC (1987) Close-chest catheter desiccation of atrioventicular junction using radiofrequency energy: a new method of catheter ablation. J Am Coll Cardiol 9:349–358
16. Huang S (1991) Advances in application of radiofrequency current to catheter ablation therapy. Pacing Clin Electrophysiol 14:28–42
17. McGahan JP, Browning PD, Brock JM, Tesluk H (1990) Hepatic ablation using radiofrequency electrocautery. Invest Radiol 25:267–270
18. Buscarini L, Rossi S, Fornari F, et al. (1995) Laparoscopic ablation of liver adenoma by radiofrequency electrocauthery. Gastrointest Endosc 41:68–70
19. Goldberg SN, Gazelle GS, Dawson SL, et al. (1995) Tissue ablation with radiofrequency: effect of probe size, gauge, duration, and temperature on lesion volume. Acad Radiol 2:399–404
20. McGahan JP, Gu WZ, Brock JM, et al. (1996) Hepatic ablation using bipolar radiofrequency electrocautery. Acad Radiol 3:418–422
21. Goldberg SN, Gazelle GS, Solbiati L, et al. (1996) Radiofrequency tissue ablation: increased lesion diameter with a perfusion electrode. Acad Radiol 3:636–644
22. Miao Y, Ni Y, Wang K, et al. (1997) Ex vivo experiment on radiofrequency liver ablation with saline infusion through a screw-tip cannulated electrode. J Surg Res 71:19–24
23. Livraghi T, Goldberg SN, Monti F, et al. (1997) Saline-enhanced radio-frequency tissue ablation in the treatment of liver metastases. Radiology 202:205–210
24. Solbiati L, Goldberg SN, Ierace T, et al. (1997) Hepatic metastases: percutaneous radio-frequency ablation with cooled-tip electrodes. Radiology 205:367–373
25. Lencioni R, Goletti O, Armillotta N, et al. (1998) Radio-frequency thermal ablation of liver metastases with a cooled-tip electrode needle: results of a pilot clinical trial. Eur Radiol 8:1205–1211
26. Goldberg SN, Stein M, Gazelle GS, et al. (1999) Percutaneous radiofrequency tissue ablation: optimization of pulsed-RF technique to increase coagulation necrosis. J Vasc Interv Radiol 10:907–916
27. Ni Y, Miao Y, Mulier S, et al. (2000) A novel "cooled-wet" electrode for radiofrequency ablation. Eur Radiol 10:852–854
28. Lees WR, Schumillian C, Gillams AR (2000) Hypotensive anesthesia improves the effectiveness of radiofrequency ablation in the liver. Radiology 217(P):228
29. Miao Y, Ni Y, Yu J, et al. (2001) An ex vivo study on radiofrequency tissue ablation: increased lesion size by using an "expandable-wet" electrode. Eur Radiol 11:1841–1847
30. Haemmerich D, Tungjitkusolmun S, Staelin ST, et al. (2002) Finite-element analysis of hepatic multiple probe radio-frequency ablation. IEEE Trans Biomed Eng 49:836–842
31. Burdío F, Güemes A, Burdío JM, et al. (2003) Bipolar saline-enhanced electrode for radiofrequency ablation: results of experimental study of in vivo porcine liver. Radiology 229:447–456
32. Lee FT Jr, Haemmerich D, Wright AS, et al. (2003) Multiple probe radiofrequency ablation: pilot study in an animal model. J Vasc Interv Radiol 14:1437–1442
33. Lorentzen T (1996) A cooled needle electrode for radiofrequency tissue ablation: thermodynamic aspects of improved performance compared with conventional needle design. Acad Radiol 3:556–563

34. Miao Yi (2000) Experimental research on radiofrequency tissue ablation as an alternative in cancer therapy Leuven, Belgium: Leuven University Press

35. Tungjitkusolmun S. Finite element modeling of radiofrequency cardiac and hepatic ablation [PhD dissertation in electrical engineering]. Madison: University of Wisconsin, 2000. Available at: http://rf-ablation.engr.wisc.edu/start_liver.html

36. Haemmerich DG. Finite element modeling of hepatic radiofrequency ablation [PhD dissertation in biomedical engineering]. Madison: University of Wisconsin, 2001. Available at: http://rf-ablation.engr.wisc.edu/start_liver.html

37. Tsai J-Z. Measurement of in vivo and in vitro swine myocardial resistivity [PhD dissertation in electrical engineering]. Madison: University of Wisconsin, 2001. Available at: http://rf-ablation.engr.wisc.edu/papers/Chanchana_Dissertation.pdf

38. Blackall JM. Respiratory motion in image-guided interventions of the liver [PhD dissertation]. London: University of London, 2002. Available at: http://www-ipg.umds.ac.uk/J.Blackall/jm_blackall_thesis.pdf

39. Tangwongsan C. Measurement of in vivo endocardial and hepatic convective heat transfer coefficient [PhD dissertation in biomedical engineering]. Madison: University of Wisconsin, 2003. Available at: http://rf-ablation.engr.wisc.edu/start_liver.html

40. Mulier S. Safe and reliable radiofrequency coagulation of liver tumors [PhD thesis in medical science]. Leuven, Belgium: Faculty of Medicine, Catholic University of Leuven

41. Lencioni R, Cioni D, Crocetti L, et al. (2003) Small hepatocellular carcinoma in cirrhosis: long-term results of percutaneous radiofrequency ablation. Radiology 229(P):411

42. Dupuy DE, Zagoria RJ, Akerley W, et al. (2000) Percutaneous radiofrequency ablation of malignancies in the lung. AJR 174:57–59

43. Vaughn C, Mychaskiw G, Sewell P, et al. (2002) Massive hemorrhage during radiofrequency ablation of a pulmonary neoplasm. Anesth Analg 94:1149–1151

44. Jeffrey SS, Birdwell RL, Ikeda DM, et al. (1999) Radiofrequency ablation of breast cancer: first report of an emerging technology. Arch Surg 134:1064–1068

45. Anzai Y, Lufkin R, DeSalles A, et al. (1995) Preliminary experience with MR-guided thermal ablation of brain tumors. AJNR 16:39–48

46. Rosenthal DI, Alexander A, Rosenberg AE, Springfield D (1992) Ablation of osteoid osteomas with a percutaneously placed electrode: a new procedure. Radiology 183:29–33

47. Rosenthal DI, Hornicek FJ, Wolfe MW, et al. (1998) Percutaneous radiofrequency coagulation of osteoid osteoma compared with operative treatment [see comments]. J Bone Joint Surg Am 80:815–821

48. Barei DP, Moreau G, Scarborough MT, Neel MD (2000) Percutaneous radiofrequency ablation of osteoid osteoma. Clin Orthop 115–124

49. Callstrom MR, Charboneau JW, Goetz MP, et al. (2002) Painful metastases involving bone: feasibility of percutaneous CT- and US-guided radio-frequency ablation. Radiology 224:87–97

50. Pinto CH, Taminiau AH, Vanderschueren GM, et al. (2002) Technical considerations in CT-guided radiofrequency thermal ablation of osteoid osteoma: tricks of the trade. AJR 179:1633–1642

51. Abraham J, Fojo T, Wood BJ (2000) Radiofrequency ablation of metastatic lesions in adrenocortical cancer [letter]. Ann Intern Med 15:312–313

52. Wood BJ, Abraham J, Hvizda JL, et al. (2003) Radiofrequency ablation of adrenal tumors and adrenocortical carcinoma metastases. Cancer 97:554–560

53. Zlotta AR, Djavan B, Matos C, et al. (1998) Percutaneous transperineal radiofrequency ablation of prostate tumour: safety, feasibility and pathological effects on human prostate cancer. Br J Urol 81:265–275

54. Beerlage HP, Thüroff S, Madersbacher S, et al. (2000) Current status of minimally invasive treatment options for localized prostate carcinoma. Eur Urol 37:2–13

55. Zlotta AR, Wildschutz T, Raviv G, et al. (1997) Radiofrequency interstitial tumor ablation (RITA) is a possible new modality for treatment of renal cancer: ex vivo and in vivo experience. J Endourol 11:251–258

56. McGovern FJ, Wood BJ, Goldberg SN, Mueller PR (1999) Radio frequency ablation of renal cell carcinoma via image guided needle electrodes. J Urol 161:599–600

57. Walther MCM, Shawker TH, Libutti SK, et al. (2000) A phase 2 study of radiofrequency interstitial tissue ablation of localized renal tumors. J Urol 163:1424–1427

58. Pavlovich CP, Walther MM, Choyke PL, et al. (2002) Percutaneous radiofrequency ablation of small renal tumors: Initial results. J Urol 167:10–15

59. Matsui Y, Nakagawa A, Kamiyama Y, et al. (2000) Selective thermocoagulation of unresectable pancreatic cancers by using radiofrequency capacitive heating. Pancreas 20:14–20

60. Dupuy DE, Hong R, Oliver B, Goldberg SN (2000) Radiofrequency ablation of spinal tumors: temperature distribution in the spinal canal. AJR 175:1263–1266

61. Lewin JS, Connell CF, Duerk JL, et al. (1998) Interactive MRI-guided radiofrequency interstitial thermal ablation of abdominal tumors: clinical trial for evaluation of safety and feasibility. J Magn Reson Imaging 8:40–47

62. Dupuy DE, Mayo-Smith WW, Cronan JJ (1999) Radiofrequency ablation in the treatment of extra-hepatic abdominopelvic malignancies. Radiology 213(P):302

63. Goldberg SN, Gazelle GS, Compton CC, et al. (1996) Radiofrequency tissue ablation of VX2 tumor nodules in the rabbit lung. Acad Radiol 3:929–935

64. Miao Y, Ni Y, Mulier S, et al. (2000) Treatment of VX2 liver tumor in rabbits with "wet" electrode mediated radio-frequency ablation. Eur Radiol 10:188–194

65. Miao Y, Ni Y, Bosmans H, et al. (2001) Radiofrequency ablation for eradication of pulmonary tumor in rabbits. J Surg Res 99:265–271

66. Lee JM, Jin GY, Li CA, et al. (2003) Percutaneous radiofrequency thermal ablation of lung VX2 tumors in a rabbit model using a cooled tip-electrode: feasibility, safety, and effectiveness. Invest Radiol 38:129–139

67. Miao Y, Ni Y, Bosmans H, et al. (2001) Radiofrequency ablation for eradication of renal tumor in a rabbit model by using a cooled-tip electrode technique. Ann Surg Oncol 8:651–657

68. Lee JM, Kim SW, Chung GH, et al. (2003) Open radio-frequency thermal ablation of renal VX2 tumors in a rabbit model using a cooled-tip electrode: feasibility, safety, and effectiveness. Eur Radiol 13:1324–1332

69. Miao Y, Ni Y, Yu J, et al. (2002) Evaluation of radiofrequency ablation as an alternative for the treatment of brain tumor in rabbits. J Neurooncol 56:119–126

70. Dickson JA, Calderwood SK (1980) Temperature range and selective sensitivity of tumors on hyperthermia: a critical review. Ann NY Acad Sci 335:180–205

71. Streffer C (1995) Molecular and cellular mechanisms of hyperthermia. In: Seegenschmiedt MH, Fessenden P, Vernon CC (eds). *Thermo-radiotherapy and thermo-chemotherapy*. Berlin: Springer, pp 47–74

72. Haines D (1993) The biophysics of radiofrequency catheter ablation in the heart: the importance of temperature monitoring. Pacing Clin Electrophysiol 16:586–591

73. Seegenschmiedt MH, Brady LW, Sauer R (1990) Interstitial thermoradiotherapy: review on technical and clinical aspects. Am J Clin Oncol 13:352–363

74. Haines DE, Watson DD, Haiperin C (1987) Characteristics of heat transfer and determination of temperature gradient and viability threshold during radiofrequency fulguration of isolated perfused canine right ventricle. Circulation 76(suppl IV):278

75. Allain JC, LeLouis M, Baily AJ, Delaunay A (1978) Isometric tension developed during heating of collagen tissues: relationships with collagen cross-linking. Biochim Biophys Acta 533:147–155

76. Grundfest WS, Litvack FI, Doyle DL, Forreater JS (1987) In: White RA (eds). *Laser in cardiovascular disease: clinical applications, alternative angioplasty devices, and guidance systems*. Chicago: Yearbook Medical Publishers, pp 32–43

77. Haines DE, Verow AF (1990) Observations on electrode-tissue interface temperature and effect on electrical impedance during radiofrequency ablation of ventricular myocardium. Circulation 82:1034–1037

78. Nath S, Haines D (1995) Biophysics and pathology of catheter energy delivery systems. Prog Cardiovasc Dis 37:185–204

79. Wissniowski TT, Hansler J, Neureiter D, et al. (2003) Activation of tumor-specific T lymphocytes by radio-frequency ablation of the VX2 hepatoma in rabbits. Cancer Res 63:6496–6500

80. Rossi S, Fornari F, Pathies C, Buscarini L (1990) Thermal lesions induced by 480 KHz localized current field in guinea pig and pig liver. Tumori 28(76):54–57

81. McGahan JP, Brock JM, Tesluk H, et al. (1992) Hepatic ablation with use of radio frequency electrocautery in the animal model. J Vasc Interv Radiol 3:291–297

82. Goldberg SN, Gazelle GS, Solbiati L, et al. (1995) Saline enhanced RF tissue ablation: demonstration of efficacy and optimization of parameters. Radiology 197(P):140

83. Goldberg SN, Gazelle GS, Halpern EF, et al. (1996) Radiofrequency tissue ablation: importance of local temperature along the electrode tip exposure in determining lesion shape and size. Acad Radiol 3:212–218

84. Boaz TL, Lewin JS, Chung YC, et al. (1998) MR monitoring of MR guided radiofrequency thermal ablation of normal liver in an animal model. J Magn Reson Imaging 8:64–69

85. Cheng YCN, Brown RW, Chung YC, et al. (1998) Calculated RF electric field and temperature distributions in RF thermal ablation: comparison with gel experiments and liver imaging. J Magn Reson Imaging 8:70–76

86. Rossi S, Di Stasi M, Buscarini E, et al. (1996) Percutaneous RF interstitial thermal ablation in the treatment of hepatic cancer. AJR 167:759–768

87. Solbiati L, Ierace T, Goldberg SN, et al. (1997) Percutaneous US guided radiofrequency tissue ablation of liver metastases: treatment and follow up in 16 patients. Radiology 202:195–203

88. Haines DE, Verow AF (1989) The impedance rise during radiofrequency ablation in vivo is prevented by maintaining an electrode tip temperature below the boiling point [abstract]. Circulation 80(suppl II):41

89. Olsrud J, Friberg B, Ahlgren M, Persson BR (1998) Thermal conductivity of uterine tissue in vitro. Phys Med Biol 43:2397–2406

90. Goldberg SN, Gazelle GS, Mueller PR (2000) Thermal ablation therapy for focal malignancy. A unified approach to underlying principles, techniques, and diagnostic imaging guidance. AJR 174:323–331

91. Jones CD, McGahan JP, Gu W, Brock JM (1995) Percutaneous liver ablation using bipolar radiofrequency electrocautery [abstract]. Radiology 197(P):140

92. Curley SA, Davidson BS, Fleming RY, et al. (1997) Laparoscopically guided bipolar radiofrequency ablation of areas of porcine liver. Surg Endosc 11:729–733

93. Le Veen RF (1997) Laser hyperthermia and radiofrequency ablation of hepatic lesions. Semin Interv Radiol 14:313–324

94. Goldberg SN, Gazelle GS, Dawson SL, et al. (1994) Radiofrequency tissue ablation using multiprobe arrays: greater tissue destruction than multiple probes operating alone. Radiology 193(P):S281

95. Goldberg SN, Gazelle GS, Dawson SL, et al. (1995) Tissue ablation with radiofrequency using multiprobe arrays. Acad Radiol 2:670–674

96. Solbiati L, Ierace T, Goldberg SN. Radiofrequency ablation of liver metastases: long-term follow-up [abstract 66]. Presented at the 7th International Congress on Interventional Ultrasound; Herlev Hospital, Denmark 3–6 September 1996

97. Hoey MF, Mulier PM, Shake JG (1995) Intramural ablation using radiofrequency energy via screw-tip catheter and saline electrode. Pacing Clin Electrophysiol 18:917

98. Livraghi T, Goldberg SN, Lazzaroni S, et al. (1995) Saline-enhanced RF tissue ablation in the treatment of liver metastases. Radiology 179(p):140. Abstract no. 70

99. Hänsler J, Neureiter D, Wasserburger M, et al. (2004) Percutaneous US-guided radiofrequency ablation with perfused needle applicators: improved survival with the VX2 tumor model in rabbits. Radiology 230:169–174

100. Miao Y, Ni Y, Mulier P, et al. (1996) Radiofrequency liver ablation with saline infusion through a screw-tip cannulated electrode. Radiology 201(P):422

101. Lee JM, Han JK, Kim SH, et al. (2003) A comparative experimental study of the in-vitro efficiency of hypertonic saline-enhanced hepatic bipolar and monopolar radiofrequency ablation. Korean J Radiol 4:163–169

102. Leveillee RJ, Hoey MF (2003) Radiofrequency interstitial tissue ablation: wet electrode. J Endourol 17:563–577

103. Goldberg SN, Ahmed M, Gazelle GS, et al. (2001) Radio-frequency thermal ablation with NaCl solution injection: effect of electrical conductivity on tissue heating and coagulation phantom and porcine liver study. Radiology 219:157–165

104. Ahmed M, Lobo SM, Weinstein J, et al. (2002) Improved coagulation with saline solution pretreatment during radiofrequency tumor ablation in a canine model. J Vasc Interv Radiol 13:717–724

105. Lobo SM, Afzal KS, Ahmed M, et al. (2004) Radiofrequency ablation: modeling the enhanced temperature response to adjuvant NaCl pretreatment. Radiology 230:175–182

106. Hoey MF, Blewett J, Nakib NA (1998) Fluoroscopic imaging of the liquid electrode perfusion into soft tissues and the developed ablations when coupled with radiofrequency energy [abstract]. Radiology 209(P):581

107. Hoey MF, Paul S, Nakib NA (1998) Saline spread and conductivity of the liquid electrode in the liver for radiofrequency energy application. Radiology 209(P):448

108. Miao Y, Ni Y, Yu J, Marchal G (2000) A comparative study on validation of a novel cooled-wet electrode for radiofrequency ablation. Invest Radiol 35:438–444

109. Haines DE, Watson DD, Verow AF (1990) Electrode radius predicts lesion radius during radiofrequency energy heating. Validation of a proposed thermodynamic model. Circ Res 67:124–129

110. Gillams AR, Lees WR. CT monitoring of contrast doped saline for perfusion radiofrequency electrodes in the ablation of liver tumours. Presented at the Annual Meeting of the Radiology Society of North American; 2003

111. Boehm T, Malich A, Goldberg SN, et al. (2002) Radiofrequency tumor ablation: Internally cooled electrode versus saline enhanced technique in an aggressive rabbit tumor model. Radiology 222:805–813

112. Denys AL, De Baere T, Kuoch V, et al. (2003) Radio-frequency tissue ablation of the liver: in vivo and ex vivo experiments with four different systems. Eur Radiol 13:2346–2352

113. Kettenbach J, Kostler W, Rucklinger E, et al. (2003) Percutaneous saline-enhanced radiofrequency ablation of unresectable hepatic tumors: initial experience in 26 patients. AJR 180:1537–1545

114. Mulier S, Ni Y, Miao Y, et al. (2003) Size and geometry of hepatic radiofrequency lesions. Eur J Surg Oncol 29:867–878

115. Goldberg SN, Gazelle GS, Solbiati L, et al. (1996) Large volume radio-frequency tissue ablation: increased coagulation with cooled-tip electrodes. Radiology 201:387

116. Haemmerich D, Chachati L, Wright AS, et al. (2003) Hepatic radiofrequency ablation with internally cooled probes: effect of coolant temperature on lesion size. IEEE Trans Biomed Eng 50:493–500

117. Weber JC, Navarra G, Jiao LR, et al. (2002) New technique for liver resection using heat coagulative necrosis. Ann Surg 236:560–563

118. Burdio F, Guemes A, Burdio JM, et al. (1999) Hepatic lesion ablation with bipolar saline-enhanced radiofrequency in the audible spectrum. Acad Radiol 6:680–686

119. Goldberg SN, Solbiati L, Hahn PF, et al. (1998) Large-volume tissue ablation with radio frequency by using a clustered internally cooled electrode technique: laboratory and clinical experience in liver metastases. Radiology 209:371–379

120. Goldberg SN, Gazelle GS, Compton CC, et al. (2000) Treatment of intrahepatic malignancy with radiofrequency ablation. Radiologic–pathologic correlation. Cancer 88:2452–2463

121. Livraghi T, Goldberg SN, Lazzaroni S, et al. (2000) Hepatocellular carcinoma: radio-frequency ablation of medium and large lesions. Radiology 214:761–768

122. Le Veen RF, Fox RL, Schneider PD, Hinrichs S (1996) Large-volume porcine liver ablation with the use of a percutaneous expandable electrosurgical probe. J Vasc Interv Radiol 7 (1 pt 2):217–218

123. Siperstein AE, Rogers SJ, Hansen PD, Gitomirsky A (1997) Laparoscopic thermal ablation of hepatic neuroendocrine tumor metastases. Surgery 122:1147–1155

124. Patterson EJ, Scudamore CH, Owen DA, et al. (1998) Radiofrequency ablation of porcine liver in vivo: effects of blood flow and treatment time on lesion size. Ann Surg 227:559–565

125. Hansen PD, Rogers S, Corless CL, et al. (1999) Radiofrequency ablation lesions in a pig liver model. J Surg Res 87:114–121

126. Scudamore CH, Shung IL, Patterson EJ, et al. (1999) Radiofrequency ablation followed by resection of malignant liver tumors. Am J Surg 177:411–417

127. de Baere T (2001) Radiofrequency ablation of the liver. AJR 177:1213–1215

128. Anai H, Uchida H, Sakaguchi H, et al. (2000) An experimental study of the radiofrequency ablation with LeVeen needle—correlation with necrotic area and the degree of the wire expansion or combined with lipiodol-transcatheter arterial embolization. Radiology 217(P):538–539

129. Kobayashi M, Ikeda K, Someya T, et al. (2002) Stepwise hook extension technique for radiofrequency ablation therapy of hepatocellular carcinoma. Oncology 63:139–144

130. Scudamore C, Buczkowski A, Patterson E, et al. (1997) Effective intraoperative radiofrequency ablation (RFA) of primary liver tumors. Asian J Surg 20:S47

131. Miao Y, Ni Y, Yu J, Marchal GJ (1999) Optimization of radiofrequency ablation by using an 'expandable-wet' electrode: results of ex vivo experiment. Radiology 213(P):102

132. Miao Y, Ni Y, Yu J, Marchal G (2000) Increased lesion in radiofrequency tissue ablation by using a novel 'expandable-wet' electrode. Acta Gastroenterol Belg 63:F1

133. Miao Y, Ni Y, Yu J, Marchal G (2000) Lesion size can be enlarged by using an 'expandable wet' electrode in radiofrequency tissue ablation. Eur Radiol 10(suppl 1):260

134. Rhim H, Kim Y, Kim Y, et al. (2000) The effect of ethanol infusion on the size of ablated lesion by radiofrequency thermal ablation: a pilot study. J Vasc Interv Radiol 11(suppl 2 pt 2):278

135. Miao Y, Ni J, Marchal G (1999) Optimization of radiofrequency ablation by using a 'cooled-wet' electrode. Eur Radiol 9(suppl 1):S50

136. Ni Y, Miao Y, Marchal G. Cooled-wet electrode. US patent no 6514251 B1, 4 February 4, 2003. Priority date 14 August 1998

137. Miao Y, Ni Y, Vaninbrouckx J, et al. (2000) Enlarged necrosis volume in radiofrequency liver tissue ablation by using a novel 'cooled-wet' electrode. Acta Gastroenterol Belg 63:F2

138. Ni Y, Miao Y, Vaninbrouckx J, et al. (2000) Radiofrequency liver tissue ablation with a 'cooled-wet' electrode: in vivo results in the swine. Radiology 217(P):229

139. Solbiati L, Goldberg SN, Livraghi T, et al. (2000) Radiofrequency thermal ablation: increased treatment effect with saline pre-treatment. Radiology 217(P):607

140. Burdio F, Guemes A, Burdio JM, et al. (2003) Bipolar saline-enhanced electrode for radiofrequency ablation: results of experimental study of in vivo porcine liver. Radiology 229:447–456

141. Schmidt D, Trubenbach J, Brieger J, et al. (2003) Automated saline-enhanced radiofrequency thermal ablation: initial results in ex vivo bovine livers. AJR 180:163–165

142. Lee JM, Kim YK, Lee YH, et al. (2003) Percutaneous radiofrequency thermal ablation with hypertonic saline injection: in-vivo study in a rabbit liver model. Korean J Radiol 4:27–34

143. Erdogan A, Grumbrecht S, Carlsson J, et al. (2000) Homogeneity and diameter of linear lesions induced with multipolar ablation catheters: in vitro and in vivo comparison of pulsed versus continuous radiofrequency energy delivery. J Interv Card Electrophysiol 4:655–661

144. McRury ID, Diamond S, Falwell G, et al. (2000) The effect of ablation sequence and duration on lesion shape using rapidly pulsed radiofrequency energy through multiple electrodes. J Interv Card Electrophysiol 4:307–320

145. RITA® System Radiofrequency Interstitial Tissue Ablation, Model 1500x user's guide and service manual. Available at: http://ritamedical.com/pdf/IFU/RF_Generators/Model_1500X_ENL.DF. Accessed 21 January 1 2004

146. Berber E, Flesher NL, Siperstein AE (2000) Initial clinical evaluation of the RITA 5-centimeter radiofrequency thermal ablation catheter in the treatment of liver tumors. Cancer J 6(suppl 4):S319–S329

147. Berchtold Elektrotom HITT® 106 Operating Instruction. Available at: http://www.berchtold.de/2/main2.htm. Accessed 21 January 2004

148. Boll DT, Lewin JS, Duerk JL, Merkle EM (2003) Do surgical clips interfere with radiofrequency thermal ablation? AJR 180:1557–1560

149. Sugimori K, Morimoto M, Shirato K, et al. (2002) Radiofrequency ablation in a pig liver model: effect of transcatheter arterial embolization on coagulation diameter and histologic characteristics. Hepatol Res 24:164

150. Morimoto M, Sugimori K, Shirato K, et al. (2002) Treatment of hepatocellular carcinoma with radiofrequency ablation: radiologic–histologic correlation during follow-up periods. Hepatology 35:1467–1475

151. Marchal G, Ni Y, Van De Mierop F, et al. (1994) Treatment of hepatic tumors in rabbits using interstitial laser therapy: how complete is destruction?. Proc SPIE 2327:234

152. Coad JE, Kosari K, Humar A, Sielaff TD (2003) Radiofrequency ablation causes thermal fixation of hepatocellular carcinoma: a post-liver transplant histopathologic study. Clin Transpl 17:377–384

153. Goldberg SN, Walovitch RC, Straub JA, et al. (1999) Radiofrequency-induced coagulation necrosis in rabbits: immediate detection at US with a synthetic microsphere contrast agent. Radiology 213:438–444

154. Goldberg SN, Saldinger PF, Gazelle GS, et al. (2000) Percutaneous tumor ablation: increased necrosis with combined radio-frequency ablation and intratumoral doxorubicin injection in a rat breast tumor model. Radiology 220:420–427

155. Goldberg SN, Kruskal JB, Oliver BS, et al. (2000) Percutaneous tumor ablation: increased coagulation by combining radio-frequency and ethanol instillation in a rat breast tumor model. Radiology 217:827–831

156. Goldberg SN, Saldinger PF, Gazelle GS, et al. (2001) Percutaneous tumor ablation: increased necrosis with combined radio-frequency ablation and intratumoral doxorubicin injection in a rat breast tumor model. Radiology 220:420–427

157. Goldberg SN, Girnan GD, Lukyanov AN, et al. (2002) Percutaneous tumor ablation: increased necrosis with combined radio-frequency ablation and intravenous liposomal doxorubicin in a rat breast tumor model. Radiology 222:797–804

158. D'Ippolito G, Ahmed M, Girnun GD, et al. (2003) Percutaneous tumor ablation: reduced tumor growth with combined radio-frequency ablation and liposomal doxorubicin in a rat breast tumor model. Radiology 228:112–118

159. Rendon RA, Kachura JR, Sweet JM, et al. (2002) The uncertainty of radio-frequency treatment of renal cell carcinoma: findings at immediate and delayed nephrectomy. J Urol 167:1587–1592

160. Neumann RA, Knobler RM, Pieczkowski F, Gebhart W (1991) Enzyme histochemical analysis of cell viability after argon laser-induced coagulation necrosis of the skin. J Am Acad Dermatol 25:991–998

161. Clark WL, Morgan JD, Asnia EJ (1924) Electrothermic methods in treatment of neoplasms and other lesions with clinical and histological observations. Radiology 2:233–246

162. Jolesz FA, Silverman SG (1995) Interventional magnetic resonance therapy. Semin Interv Radiol 12:20–27

163. Lewin JS, Connell CF, Duerk JL, et al. (1998) Interactive MRI-guided radiofrequency interstitial thermal ablation of abdominal tumors: clinical trial for evaluation of safety and feasibility. J Magn Reson Imaging 8:40–47

164. Quesson B, de Zwart JA, Moonen CTW (2000) Magnetic resonance temperature imaging for guidance of thermotherapy. J Magn Reson Imaging 12:525–533

165. Gazelle GS, Goldberg SN, Solbiati L, Livraghi T (2000) Tumor ablation with radio-frequency energy. Radiology 217:6333–6346

166. Gillams AR (2001) Thermal ablation of liver metastases. Abdom Imaging 26:361–368

167. Dupuy DE, Goldberg SN (2001) Image-guided radiofrequency tumor ablation: challenges and opportunities. II. J Vasc Interv Radiol 12:1135–1148

168. Kruskal JB, Oliver B, Huertas JC, Goldberg SN (2001) Dynamic intrahepatic flow and cellular alterations during radiofrequency ablation of liver tissue in mice. J Vasc Interv Radiol 12:1193–1201

169. Cha CH, Lee FT Jr, Gurney JM, et al. (2000) CT versus sonography for monitoring radiofrequency ablation in a porcine liver. AJR 175:705–711

170. Anzai Y, Lufkin R, Desalles A, et al. (1995) Preliminary experience with MR-guided thermal ablation of brain tumors. AJNR 16:39–48

171. Lewin JS, Connell CF, Duerk JL, et al. (1998) Interactive MRI-guided radiofrequency interstitial thermal ablation of abdominal tumors: clinical trial for evaluation of safety and feasibility. J Magn Reson Imaging 8:40–47

172. Livraghi T, Goldberg SN, Meloni F, et al. (1999) Hepatocellular carcinoma: comparison of efficacy between percutaneous ethanol instillation and radiofrequency. Radiology 210:655–661

173. Meloni MF, Goldberg SN, Livraghi T, et al. (2001) Hepatocellular carcinoma treated with radiofrequency ablation: comparison of pulse inversion contrast-enhanced harmonic sonography, contrast-enhanced power Doppler sonography, and helical CT. AJR 177:375–380

174. Boehm T, Malich A, Goldberg SN, et al. (2002) Radio-frequency ablation of VX2 rabbit tumors: assessment of completeness of treatment by using contrast-enhanced harmonic power Doppler US. Radiology 225:815–821

175. Choi D, Lim HK, Lee WJ, et al. (2003) Early assessment of the therapeutic response to radio frequency ablation for hepatocellular carcinoma: utility of gray scale harmonic ultrasonography with a microbubble contrast agent. J Ultrasound Med 22:1163–1172

176. Varghese T, Techavipoo U, Liu W, et al. (2003) Elastographic measurement of the area and volume of thermal lesions resulting from radiofrequency ablation: pathologic correlation. AJR 181:701–707

177. Li KPC, Jeffrey RB Jr, Kandil A, et al. (1993) Experimental hepatic tumor necrosis: comparison of spin-echo and pulsed magnetization transfer contrast magnetic resonance imaging. Invest Radiol 28:896–902

178. Ni Y, Marchal G, Herijgers P, et al. (1996) Paramagnetic metalloporphyrins: from enhancers for malignant tumors to markers of myocardial infarcts. Acad Radiol 3:S395–S397

179. Marchal G, Ni Y. Use of porphyrin-complex or expanded porphyrin-complex as an infarction localization diagnosticum. US patent no. 6,013,241, 11 January 2000. Priority date 23 January 1995

180. Ni Y, Cresens E, Adriaens P, et al. (2002) Necrosis avid contrast agents: introducing nonporphyrin species. Acad Radiol 9(suppl 1):S98–S101

181. Ni Y, Bormans G, Marchal G, Verbruggen A. Tissue infarction and necrosis specific compounds (of hypericin derivatives). UK patent application no. LRD-GB-1-455. Priority date 25 July 2003

182. Ni Y, Marchal G, Yu J, et al. (1995) Localization of metalloporphyrin induced "specific" enhancement in experimental liver tumors: a comparison between MRI, microangiographic and histologic findings. Acad Radiol 2:687–699

183. Ni Y, Petré C, Miao Y, et al. (1997) Magnetic resonance imaging-histomorphologic correlation studies on paramagnetic metalloporphyrins in rat models of necrosis. Invest Radiol 32:770–779

184. Ni Y, Adzamli K, Miao Y, et al. (2001) MRI Contrast enhancement of necrosis by MP-2269 and Gadophrin-2 in a rat model of liver infarction. Invest Radiol 36:97–103

185. Ni Y, Marchal G, Petré C, et al. (1994) Metalloporphyrin enhanced magnetic resonance imaging of acute myocardial infarction. Circulation 90(pt 2):I-468

186. Ni Y, Bormans G, Marchal G, Verbruggen A. Patent application: Tissue infarction and necrosis specific compounds (of hypericin derivatives). Ref No. LRD-GB-1-455. Priority date July 25, 2003. The Patent Office, UK, International Patent Cooperation treaty, PCT/BE2004/000107.

187. Marchal G, Ni Y, Herijgers P, et al. (1996) Paramagnetic metalloporphyrins: infarct avid contrast agents for diagnosis of acute myocardial infarction by magnetic resonance imaging. Eur Radiol 6:2–8

188. Herijgers P, Laycock SK, Ni Y, et al. (1997) Localization and determination of infarct size by Gd-mesoporphyrin enhanced MRI in dogs. Int J Card Imaging 13:499–507

189. Ni Y, Pislaru C, Bosmans H, et al. (1998) Validation of intracoronary delivery of metalloporphyrin as an in vivo "histochemical staining" for myocardial infarction with MR imaging. Acad Radiol 5(suppl 1):S37–S41

190. Pislaru S, Ni Y, Pislaru C, et al. (1999) Noninvasive measurements of infarct size after thrombolysis with a necrosis-avid MRI contrast agent. Circulation 99:690–696

191. Ni Y, Pislaru C, Bosmans H, et al. (2001) Intracoronary delivery of Gd-DTPA and gadophrin-2 for determination of myocardial viability with MR imaging. Eur Radiol 11:876–883

192. Ni Y, Miao Y, Bosmans H, et al. (1997) Evaluation of interventional liver tumor ablation with Gd-mesoporphyrin enhanced magnetic resonance imaging. Radiology 205:319

193. Ni Y, Cresens E, Adriaens P, et al. (2002) Exploring multifunctional features of necrosis avid contrast agents. Acad Radiol 9(suppl 2):S488–S490